The Applications of PET in Clinical Oncology

Ludwig G. Strauss and Peter S. Conti

Institute of Radiology and Pathophysiology, German Cancer Research Center, Heidelberg, Germany and Department of Radiology and Radiological Sciences, The Johns Hopkins Medical Institutions, Baltimore, Maryland

With the advent of a new generation of PET scanners that have introduced whole-body PET to the clinical setting, there is now more interest in developing protocols for the evaluation of both intracranial and somatic cancers. The value of PET in clinical oncology has been demonstrated with studies in a variety of cancers including colorectal carcinomas, lung tumors, head and neck tumors, primary and metastatic brain tumors, breast carcinoma, lymphoma, melanoma, bone cancers, and other soft-tissue cancers. A summary of current clinical applications of PET in oncology is presented with special attention to colorectal, lung, and intracranial neoplasms since the majority of clinical trials have focused on these cancers. A variety of radiopharmaceuticals are described that are currently included in clinical tumor-imaging protocols, including metabolic substrates such as fluorine-18-fluorodeoxyglucose and carbon-11-methionine, and analogs of chemotherapeutic agents such as fluorine-18-fluorouracil and fluoroestradiol. An attempt is also made to include examples of clinical trials that demonstrate response to therapeutic intervention. The increasing number of oncologic PET studies reflects the growing interest in functional imaging in oncology.

J Nucl Med 1991; 32:623–648

The ability to identify structural alterations in diseased tissues, such as those seen in cancer, has increased dramatically in the last two decades with the development of noninvasive cross-sectional imaging techniques including computed tomography (CT) and magnetic resonance imaging (MRI). Whereas significant advances have been made in morphologic imaging, less attention has been given, until recently, to the development of in vivo methods of quantitating functional metabolism in normal and diseased tissues (1). Positron emission tomography (PET) is one example of such a technique that has the potential to yield the physiologic information necessary not only to provide a means for diagnosis of cancers based on altered tissue metabolism, but also to serve as a tool for monitoring the effects of the therapy on tissue metabolism. Correlative functional-anatomical imaging will permit the study of metabolic processes in the anatomic loci where they occur and perhaps detect changes indicative of tumor

response to therapy before alterations in structures occur.

PET studies of tumors can be performed for several reasons including:

1. Quantification of tumor perfusion.
2. Evaluation of tumor metabolism.
3. Tracing of radiolabeled cytostatic agents.

The quantification of tumor perfusion requires the use of nonmetabolized radiolabeled tracers and permits the determination of the tissue perfusion. Different radiopharmaceuticals had previously found use for perfusion studies (Table 1). Multiparameter studies necessitate the application of short-lived isotopes; therefore, oxygen-15- (^{15}O) labeled radiopharmaceuticals have found preferential use. Generator-produced copper compounds are also gaining interest (2). PET studies of the tumor metabolism are primarily performed with glucose derivatives and amino acids (Table 2). For practical reasons fluorine-18-deoxyglucose ([^{18}F]FDG) has found widespread use in PET and is the standard radiopharmaceutical for metabolic studies, particularly in the brain (3). Other tracers like carbon-11-(^{11}C) methionine, ^{11}C-labeled thymidine, and ^{11}C-tyrosine are under investigation at different PET centers (4–13). The evaluation of the pharmacodynamics and kinetics of cytostatic agents requires the radiolabeling of such drugs. Thus far, only a small number of labeled cytostatic drugs have been found useful for PET studies (14–17).

Since tumor heterogeneity is a well-known accepted concept among tumor biologists, it is likely that imaging techniques designed to evaluate cancers will need to account for that variability expressed as differences in macroscopic anatomy and metabolism. Multiple radiotracers will eventually be necessary to adequately evaluate these lesions for diagnosis as well as for the monitoring of therapeutic responses.

METHODS USED AT THE AUTHORS' INSTITUTIONS

Imaging Devices

At the German Cancer Research Center, a positron-emission tomograph (PC2048-7WB, Scanditronix Co.) with two ring detectors is used for PET examinations. The system provides for the simultaneous acquisition of three slices, two primary sections and one cross section. Each of the two 107-cm rings contains 512 BGO/GSO detectors (crystal size 6 mm × 20 mm × 30 mm) and provides a field of view of 52 cm. The mean sensitivity for the two primary sections is 12,500 cps per μCi/cm^3 and 17,500 cps

TABLE 1
Radiopharmaceuticals Used for PET Studies in Tumor
Patients

Radiopharmaceutical	Study type
$H_2^{15}O$	Perfusion
$C^{15}O_2$	Perfusion
$C^{15}O$	Blood volume
$^{11}CO_2$	Perfusion
^{11}CO	Blood volume
^{11}C-butanol	Perfusion
^{82}Rb	Perfusion
^{11}C-aminocyclopentanecarboxylic acid (ACPC)	Amino acid uptake (L-type)
^{11}C-aminoisobutyric acid (AIB)	Amino acid uptake (A-type)
^{11}C-methionine	Uptake, metabolism
^{11}C-thymidine	Metabolism, proliferation
^{11}C-tyrosine	Metabolism
^{13}N-ammonia	Perfusion
^{13}N-glutamate	Uptake, metabolism
^{18}F-FDG	Glucose transport, phosphorylation
^{18}F-deoxyuridine	Metabolism
^{18}F-tyrosine	Metabolism
^{18}F-uracil (FU)	Uptake, metabolism
^{18}F-uridine (FUrd)	Metabolism, proliferation

per μCi/cm^3 for the secondary slice. The dead-time loss is 10% at 30,000 cps per slice. The evaluation of spatial linearity shows that the maximum displacement from the ideal source position is less than 0.4 mm in the whole field of view. Transmission scans with more than 15 million cps were obtained before the radionuclide application to obtain cross-sections for the attenuation correction of the acquired images.

The CTI NeuroECAT, a three-ring, five-slice brain-only PET scanner, is currently in use at The Johns Hopkins Medical Institutions. Each "ring" is an octagon of 88 BGO detectors. Removable "shadow shields" control in-plane resolution; removable septa control axial resolution. All scans are acquired from direct slices only (i.e., no cross-slice data), with shadow shields and septa in place. This produces in-plane resolution of 8 mm, and axial resolution of 14 mm FWHM; sensitivity is 10,000 cps/μCi/cc. Raw projection data are corrected for individual detector sensitivity variation and attenuation (with an ellipse placed around a first-order reconstruction).

Analysis of Radiotracer Accumulation

Several techniques may be used to express the accumulation of radiotracers in tissue. A semiquantitative analysis of tracer accumulation in normal tissues and

TABLE 2
Therapeutic Protocol for Patients with Unresectable
Recurrent Carcinomas (n = 8)

Cytostatic Agent	5-FU, 750 mg/m^2 body surface area
Application	Continuous infusion (aa. iliacae int.)
Schedule	5 days
Radiation therapy	4*2.5 Gy/cycle

tumors is used by many investigators studying somatic lesions. A number of terms have been given to the value calculated by this method, including DAR (distribution activation ration), SUV (standardized uptake value), and DUR (differential uptake ratio). These calculations are generally based on the following ratio, which relates activity found in the tissue to the dose injected and the subject's mass (*18*):

$$\frac{\text{cmp found per g tissue}}{\text{cmp injected per g subject mass}}.$$

This has been described as a method of expressing biologic tissue distribution or relative concentration of radiotracers following i.v. administration in a variety of species (*18*).

While some investigators have attempted direct metabolic analysis of radiotracer activity, such as calculation of regional glucose values with [^{18}F]FDG in cancers of the body, this methodology is most commonly utilized in intracranial studies. However, the techniques are frequently limited when tumor tissue is evaluated because many of the parameters required for proper mathematical modeling of these biological processes are unknown; for example, the value of the lumped constant in modeling regional glucose metabolism using [^{18}F]FDG in neoplasms. For this and other reasons, many investigators rely more on simple ratio analyses that directly compare abnormal tissue to surrounding or distant normal sites, or on visual inspection, particularly in limited clinical examinations of intracranial lesions.

COLORECTAL TUMORS

Diagnosis of Tumor Recurrence

The colorectal tumor is one of the most common tumors in oncology. Abdominoperineal resection of colorectal carcinoma is followed by local recurrence in 25%–30% of all patients within 2 yr after surgery (*19*). The differentiation between recurrent tumor and scar is the major problem in the treatment of these patients. Computed tomography (CT) does not permit reliable differentiation of these soft-tissue masses, as shown by Grabbe and Winkler, who reviewed the data on 51 patients with local tumor recurrence (*20*). They found that the combination of carcinoembryonic antigen (CEA) levels and rectoscopy was more effective in enabling this differentiation than CT, conventional diagnostic studies, and/or clinical examination (*20*). T1 and T2 MRI also appears to be of limited use as demonstrated by Johnson et al. (*21*). The accuracy of immunoscintigraphy (IS) is variable and is dependent on the localization and size of the questionable lesion (*22*). The diagnostic problems encountered in the evaluation of possible tumor recurrence may be studied with PET, since such examinations can provide information about the metabolism of mass lesions.

FDG, one of the most common PET radiopharmaceu-

ticals, was used in a study to differentiate tumor from scar lesions on the basis of local glucose metabolism measurements in 33 patients. The perfusion of the space-occupying lesions was evaluated with ^{15}O-labeled water. Only patients with masses exceeding 1.5 cm in diameter were included in the study. Twenty-three patients had at least one biopsy result suggestive of tumor recurrence, whereas 10 patients had histologically proven scar lesions. Computed tomography was used to localize the largest lesion diameter immediately prior to the PET study.
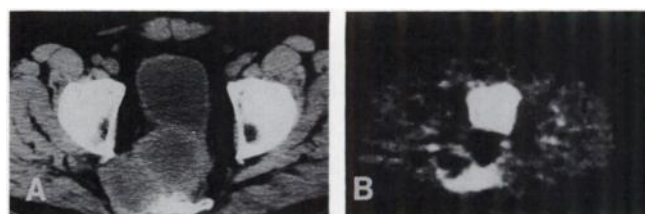
Following transmission scanning, 2960–3700 MBq of ^{15}O-labeled water was injected and five 1-min images were acquired. This was followed by the administration of 111–440 MBq FDG and acquisition of twelve 5-min images. PET cross-sections were reconstructed using an interactive method with scatter and attenuation correction (23). Regions of interest (ROIs) were placed over the lesion as well as over the gluteal muscles, which served as normal references. The tracer uptake was expressed as standardized uptake values (SUV):

$$SUV = \frac{\text{tissue concentration (mCi/g)}}{\text{injected dose (mCi)/body weight (g)}}.$$

All tumors were visible in the PET slices following intravenous FDG injection (Fig. 1), while the FDG uptake was low in scars. One patient with a scar also had a lymph node metastasis in the left inguinal region, which was demonstrated in PET with high FDG uptake (Fig. 2). The FDG uptake in the malignant lesions 1 hr after radiotracer application was more than twice as high as in normal soft tissue (Fig. 3). The quantitative evaluation of the FDG uptake demonstrates that tumor and scar lesions can be differentiated on the basis of PET measurements (Fig. 4). Only one tumor lesion was misclassified due to low tracer accumulation. We noted a low correlation (r = 0.55) between the uptake of ^{15}O-labeled water and the FDG accumulation in tumors (Fig. 5). The evaluation of these data demonstrates that perfusion studies are not adequate for tumor differentiation and that information about the tumor metabolism is required to classify unknown masses.

FDG has been used in several experimental studies (24, 25). Goodman et al. demonstrated rapid FDG uptake in rats with implanted glioma (26). Similar results were reported by Paul et al., who noted high FDG accumulation in canine osteosarcoma and mammary carcinoma (27). Our results in patients with colorectal tumors are comparable with the experimental findings. A correlative study with PET and immunoscintigraphy was performed by Als et al. (28). The authors report on the evaluation of 10 patients, who were examined with FDG and ^{99m}Tc-labeled monoclonal antibody for CEA. The sensitivity was high for both methods; however, problems existed with PET due to high residual bladder activity.

The artifacts related to excreted FDG were significantly reduced in our study due to the application of an iterative reconstruction technique (23). The iterative technique
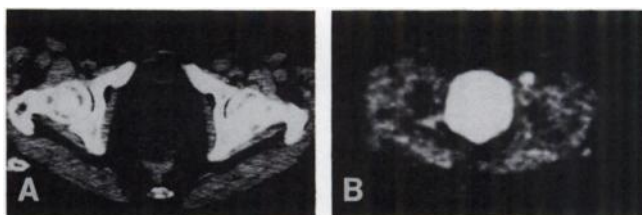

FIGURE 1. (A) CT Image of a large colorectal tumor infiltrating the os sacrum. (B) PET image 1 hr after i.v. injection of FDG. Increased tracer uptake in the peripheral parts of the tumor and in the os sacrum due to the tumor infiltration. Note the low tracer concentration in the central tumor region suggestive of tumor necrosis.

results in less artifacts, especially if high-activity concentrations (e.g., excreted tracer in the bladder) are present (Fig. 6), and is recommended when accurate PET measurements of tracer uptake are required for diagnosis.
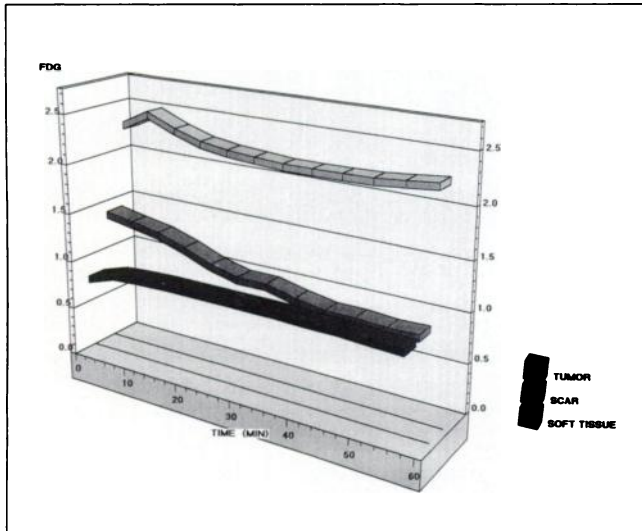
Increased FDG uptake also may be present in inflammatory lesions. Fukuda et al. performed FDG studies in tumor-bearing rats and rabbits and reported the accumulation of FDG to be significantly higher in tumors than in inflammatory disease (29). However, our data in one patient with an inflammatory mass demonstrate that inflammation may obscure tumor detection, particularly if a patient had received radiation therapy. Therefore, clinical data must be included in the PET evaluation. In summary, we believe that PET with FDG provides significant information about the differentiation of colorectal recurrency and scar.

Therapy Management with PET

Radiation therapy has been used for palliative treatment of nonresectable, loco-regional recurrence of colorectal carcinomas (19,30–32). A palliative effect is generally achieved with 35-45 Gy, whereas higher doses do not improve the response. The combination of radiation therapy and regional fluorouracil- (5-FU) chemotherapy has been used for the treatment of local recurrences. A partial tumor regression was achieved in 15% of the patients, while a palliative result was obtained in 48% (33). We evaluated the effect of a mixed-beam schedule, based on a combination of 40 Gy photons and 10 Gy neutrons, on
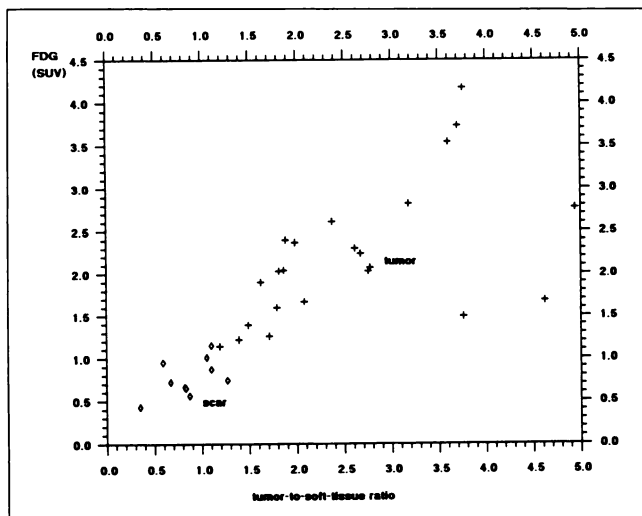

FIGURE 2. (A) Questionable soft-tissue lesion dorsal to the bladder. (B) PET FDG image at the level of the CT. Low tracer accumulation dorsal to the bladder is indicative of scar tissue. Focal uptake in the left inguinal region was confirmed as a lymph node metastasis, while the soft-tissue lesion near the bladder was scar tissue.
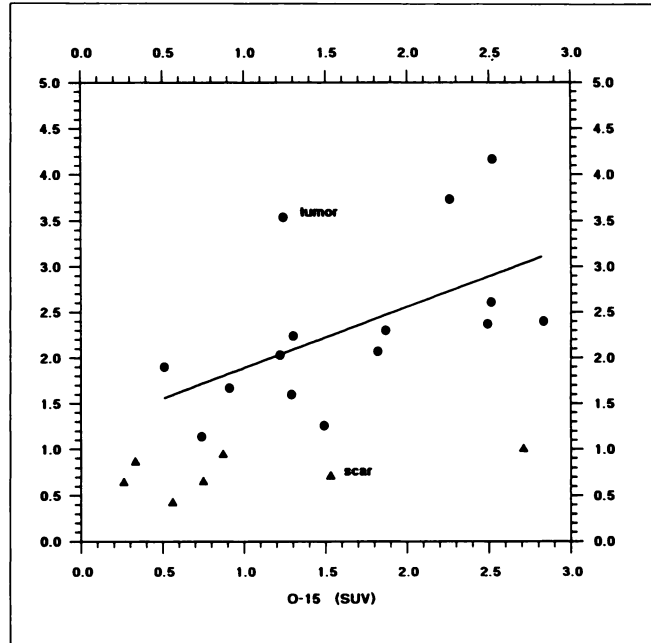
FIGURE 3. Time-activity curves (mean values) up to 1 hr after intravenous FDG injection. The uptake is expressed as standardized uptake values. Increased, nearly constant uptake of FDG was seen in the tumors (n = 23), while FDG accumulation in the scar tissue (n = 10) was increased up to 40 min postinjection and then constant and comparable to the normal muscle tissue.

tumor blood-flow and metabolism. Only patients without pretreatment (radiation therapy or chemotherapy) were directed to the mixed-beam protocol. Using ^{18}F-labeled FDG, we assessed whether PET would give additional information about the change in tumor metabolism before, during, and after radiation therapy. Oxygen-15-labeled water was used in selected patients to obtain data about the tumor perfusion.

Seventeen patients with an unresectable, locally recurrent rectosigmoidal malignancy were directed to radiation therapy. A mixed-beam protocol was used (40 Gy photons, up to 10 Gy neutrons) for the radiation treatment. No
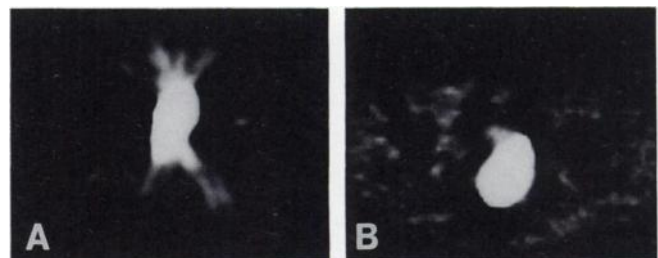

FIGURE 4. Tumor-to-soft-tissue ratios and FDG SUV values in 10 scar lesions and 23 recurrent carcinomas. An overlap of the SUV was seen in only one tumor patient.

FIGURE 5. Perfusion and metabolism in 7 scar lesions and 15 colorectal tumors. A low correlation coefficient of 0.55 was noted for the tumors, while no correlation was observed for the scars. The data demonstrate that perfusion measurements fail to differentiate between benign and malignant tissue.

patients were previously treated with radiation or chemotherapy. PET results did not influence the diagnostic and therapeutic modalities that were used in these patients. Radiation therapy followed immediately after the first PET examination. Follow-up PET studies were performed up to 603 days after onset of radiotherapy. The results of PET were compared with preexisting clinical data. Forty-seven studies were performed with ^{15}O-labeled water (2331–3700 MBq, 80–100 mCi) prior to the FDG application, while 67 examinations were carried out with 126–440 MBq (3–12 mCi) of FDG.

All colorectal recurrences were visible in the PET FDG images before radiation therapy. A significant decrease in the FDG accumulation was noted after combined treat-
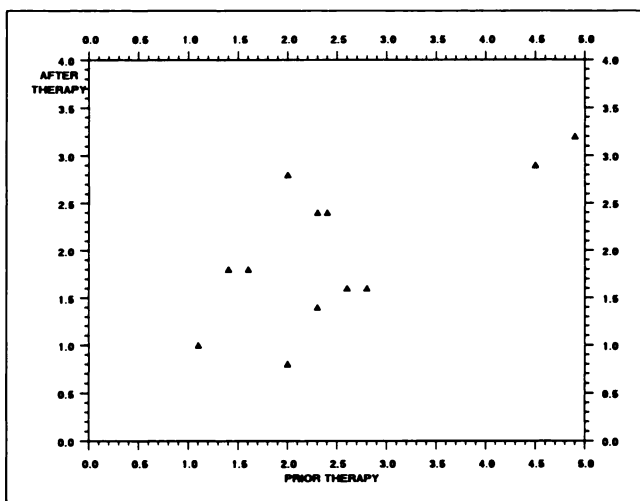

FIGURE 6. (A) PET cross section of the pelvic region. The image was reconstructed using the filtered backprojection algorithm provided by the manufacturer. Severe artifacts are due to excreted FDG in the bladder. (B) The same data were reconstructed with an iterative algorithm yielding a significant reduction in reconstruction artifacts. Only the iterative image reconstruction can be used for a qualitative and quantitative evaluation of the PET data.

ment in 12 patients (Fig. 7). The FDG uptake decreased in 69% of the patients after the photon therapy, while a further decrease in tumor metabolism was noted after neutron therapy in only 27%. More than three follow-up PET studies were performed in 11 of 17 patients. Tracer concentrations decreased 30–60% within 60 days after onset of mixed-beam radiation therapy in 6 of the 11 patients. While the FDG uptake was lower after radiation therapy, we noted FDG concentration values comparable to normal soft tissue in 5 of 11 patients. In Figure 8, a long term follow-up study is shown in a patient with recurrent colorectal malignancy. The PET study prior to radiotherapy reveals a large tumor infiltrating the os sacrum. Seven months after radiotherapy a low but significant FDG uptake is noted in the peripheral part of the tumor, indicative of residual tumor metabolism.

Further follow-up studies documented local tumor progression and multiple lung metastases. The FDG uptake in the tumor region remained abnormal, while the CEA was within normal limits up to 300 days after therapy. No correlation was obtained for CEA values and FDG concentrations in the tumor (Fig. 9). In 15 of 43 examinations normal CEA levels were associated with increased FDG uptake, whereas increased CEA and normal FDG concentrations were seen in only 2 studies (normal range SUV <1.0).

The results demonstrate that PET with FDG can document the change in FDG uptake in colorectal tumors using radiation therapy. While a complete or incomplete palliative effect was achieved in all patients, a significant decrease of FDG concentration values was noted in only 6 of 11 patients. Ogawa et al. studied five patients with cerebral gliomas before, during, and after combined treatment with radiation therapy and chemotherapy (34). They reported a decrease in tumor metabolism in four of five patients within 1 mo after treatment. Thus, differences in
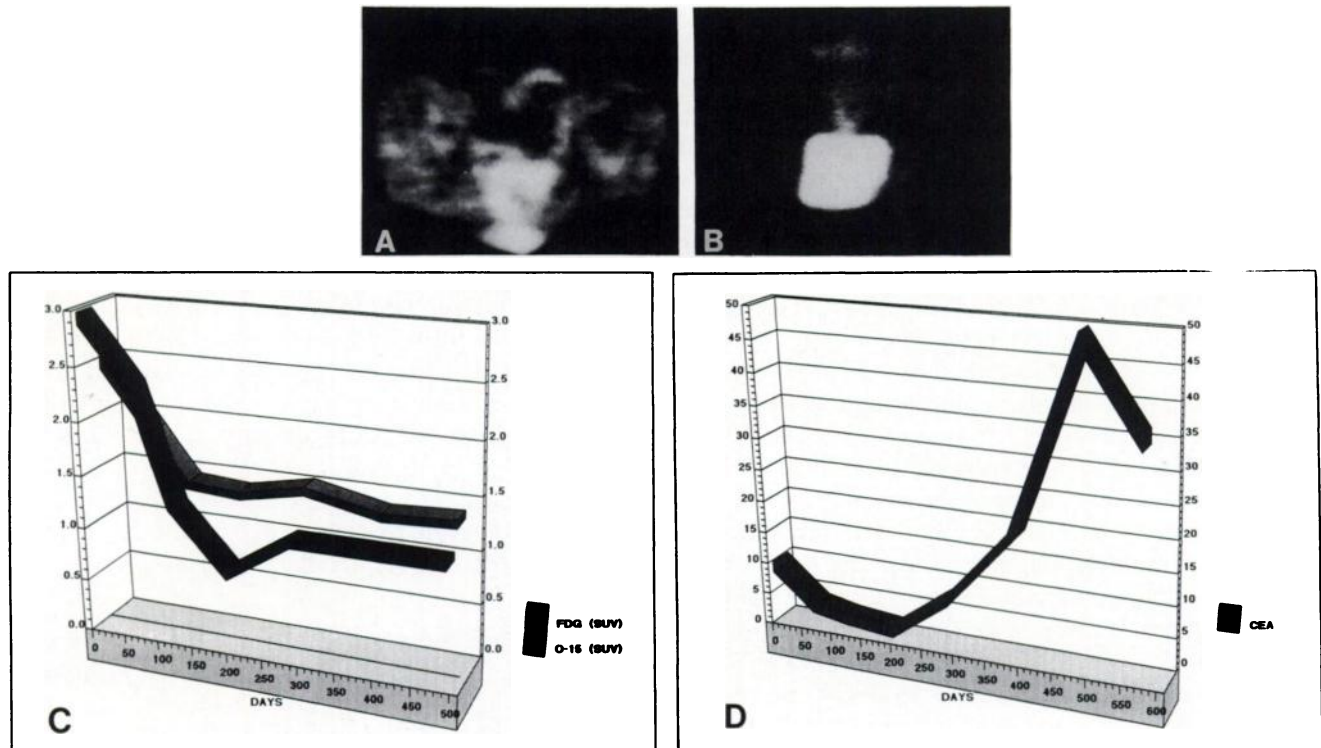
response to therapy may depend on the various tumor types as well as the different protocols used for therapy.

Measurements of CEA concentrations in plasma have been widely used in the follow-up of patients with colon tumors (35). While all patients in our study had colorectal malignancies, CEA levels were within normal range in 14 of 41 examinations before and after radiotherapy. FDG concentration values were normal in only 4 of the 41 studies. Therefore, the measurement of FDG uptake in patients with colorectal tumors is a more sensitive parameter than CEA, particularly when tumor response to therapy is evaluated. These data are in agreement with results reported from Kimball et al., who isolated a tumor subpopulation in which CEA production could not be noted (36). Furthermore, this cell line was resistant to 5-FU and multiple metastases were found. These data suggest that metabolic studies are required to detect residual metabolic activity in patients if further therapy is considered.

Combined Treatment with Radio- and Chemotherapy

Recurrent rectal carcinomas and unresectable colorectal tumors raise many therapeutic problems. Radiation therapy can result in tumor palliation (19), while systemic chemotherapy of large-bowel tumors remains disappointing (37). 5-Fluorouracil and its derivatives still continue to be the most commonly used cytostatic agents for this malignancy (37). It has long been hoped that regional chemotherapy with intraarterial administration of cytostatic agents would improve therapeutic outcome. This approach has been combined with simultaneous radiation therapy in unresectable primary tumors and recurrent rectal carcinomas. Shani and Wolf showed in an animal study that drug-responsive tumors had a 20:1 tumor-to-blood ratio 12 hr postinjection, whereas drug-resistant tumors had only a 4:1 ratio (38). These data indicate that FU uptake measurements in tumor tissue may be helpful to predict response to FU chemotherapy in patients. Patients have been examined in our laboratory with ^{18}F-labeled FU to obtain quantitative data about the uptake of FU and the metabolism and perfusion of colorectal tumors. These data were compared also with tumor perfusion, shunting, and ^{13}N-glutamate distribution.
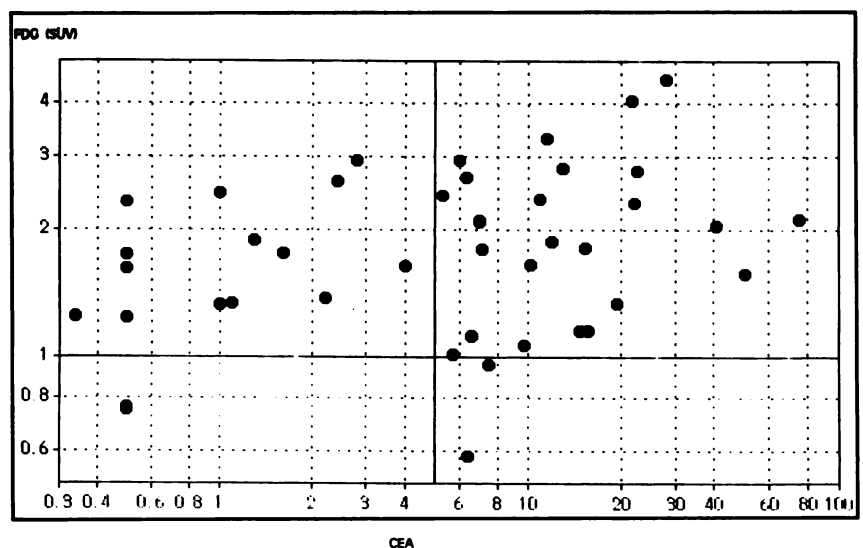
All eight patients included in this study had large recurrent rectal carcinomas. A total of 17 examinations were performed. For intraarterial chemotherapy a 7-F-catheter was inserted into each internal iliac artery. All patients were examined prior to the chemotherapeutic cycle. Three cycles of chemotherapy and radiation therapy were performed. Each chemotherapeutic cycle was separated from the next by 4 wk. Radiation therapy was simultaneously performed during chemotherapy. Details of the therapeutic schedule are shown (Table 2). We used angiography and CT, as well as different radioisotope procedures, to evaluate shunting, metabolic turnover, and FU accumulation prior to the intra-arterial chemotherapeutic cycle (Table 3).

FIGURE 7. FDG uptake values prior to and after combined treatment (n = 12). Significant reduction of tracer uptake was seen in six patients.

FIGURE 8. (A) PET cross section of a recurrent colorectal tumor prior to radiation therapy. Increased tumor metabolism and infiltration of the os sacrum. (B) PET cross-section 7 mo after radiotherapy. Residual tumor metabolism in the peripheral parts of the mass and in the os sacrum. The PET findings were indicative of tumor recurrence, which was confirmed by the clinical follow-up. (C) FDG SUV values and perfusion values of the same patient. Note the drop in FDG uptake in response to therapy. The FDG values were increased in all PET studies as compared to normal soft tissue, while the perfusion values were low. (D) CEA plasma levels were abnormal more than 300 days after onset of therapy due to a second tumor recurrence. The data show that the FDG uptake values were more sensitive than CEA.

The SPECT perfusion studies were obtained following separate intraarterial infusion of 185 MBq ^{99m}Tc-MAA into each catheter placed in the internal iliac arteries. Tomographic sections of the pelvic region were reconstructed and the relative tumor blood-flow was calculated. Tumor shunting was assessed using posterior views of the pelvis and the lung. Immediately after intraarterial injection of 185–370 MBq ^{13}N-glutamate, several images were obtained with a time interval of 8 min. Total examination time was 45 min. In selected patients, PET cross sections were acquired following ^{13}N-glutamate injection up to 30 min postinjection. Following the ^{13}N-glutamate study, we

FIGURE 9. CEA plasma levels and FDG uptake values in 43 PET studies. In 15 of 43 examinations normal CEA levels were associated with increased FDG uptake values.

TABLE 3
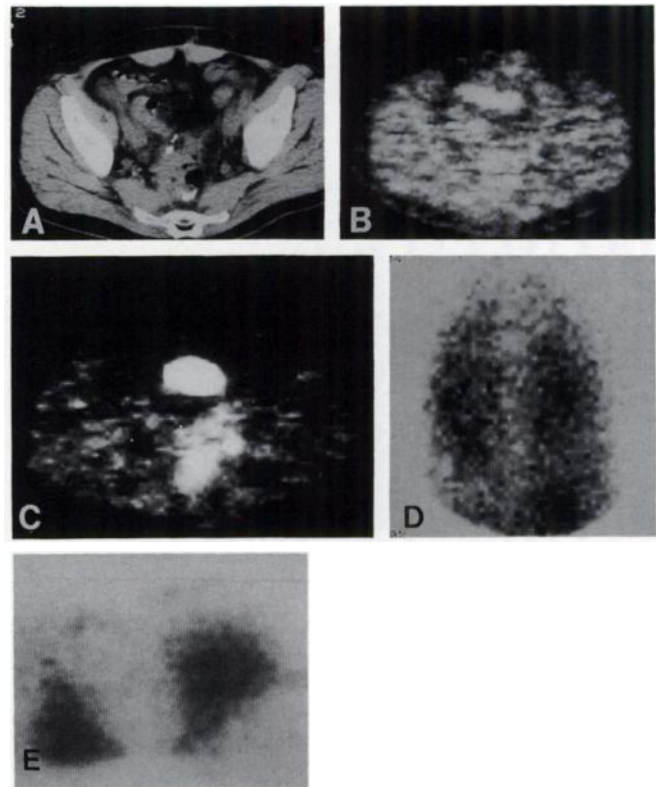Imaging Modalities Used for Intraarterial Chemotherapy and Radiation Therapy of Rectum Carcinomas

Method	Region	Comment
Angiography	Pelvis	Tumor blood supply
CT	Pelvis	Tumor staging
99mTc-MAA (SPECT)	Pelvic, lung	Perfusion, shunting
13N-glutamate	Pelvis, whole body	Tumor metabolism
18F-FU	Pelvis, whole body	FU uptake

injected 148–222 MBq 18F-labeled fluorouracil through the catheters. Scanning started immediately after the injection, and continued for 45 min on average. The 13N-glutamate and 18F-FU accumulation was evaluated using ROIs, and was expressed as a percent of the total dose. Following intraarterial administration of tracer, only the first scans were used for this assessment to evaluate the tracer transport.

We were able to compare the intravenous and intraarterial administration of FU in a patient receiving combined treatment (Fig. 10). Whereas the PET image 2 hrs after i.v. FU injection shows a nearly homogenous distribution of the 18F activity, an increased 18F accumulation was noted following intraarterial administration. The SPECT perfusion study showed that 38% of the injected particles were found in the tumor region, indicative of high tumor perfusion. The shunting fraction was 9%. Despite selective injection, only 12% of the administered 18F-FU was detected in the target area. Most of the 18F activity was noted in the liver. This example demonstrates that even a high, preferential perfusion of the tumor does not lead to a high FU uptake.

An evaluation of 17 examinations demonstrates that tumor perfusion was below 10%, while tumor shunting and 13N-glutamate accumulation were between 5% and 15% of the injected dose. Median perfusion was 8% and median shunt value was 10% (Table 4). The percentage of 18F-FU accumulation in the tumor region was a function of tumor perfusion and glutamate uptake, as demonstrated in Figure 11 (r = 0.80).

Intraarterial administration of antitumor drugs has been widely used in cancer therapy. The combination of intraarterial chemotherapy with radiation therapy is recommended (33). We combined FU chemotherapy with radiation therapy (10 Gy per cycle) to enhance the antitumor effects of the cytostatic agent. The potential benefits of this combination are being assessed in an ongoing study. The intra-arterial injection of FU should increase the cytostatic concentration in tumor tissue and result in lower systemic effects due to first pass extraction and higher local dose of the cytostatic agent. Wile et al. injected FU into a surgically isolated pelvic circuit during hyperthermic perfusion and found a 7–8-fold greater pelvic drug concentration than that observed in the systemic compartment (39). The transcatheter occlusion of both the superior and inferior gluteal arteries was used by Woods et al. to direct blood
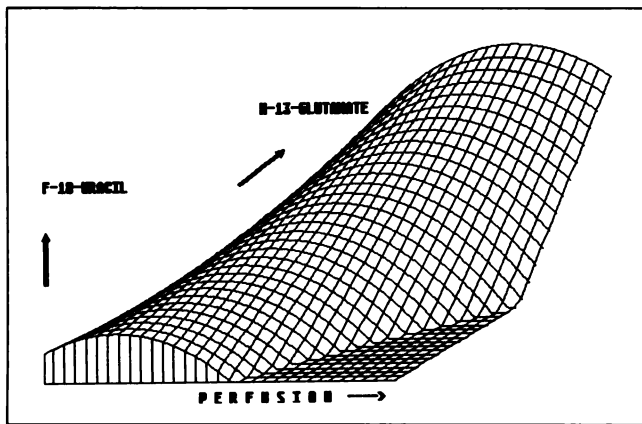

FIGURE 10. (A) CT image of a recurrent colorectal tumor prior to therapy. (B) PET cross section at the level of the CT image in Figure 10A. The image demonstrates the 18F distribution 2 hr after i.v. infusion of 18F-labeled fluorouracil. Note nearly homogenous tracer distribution. (C) This PET cross-section was obtained 2 hr after intraarterial FU infusion. Significantly higher tracer uptake in the tumor region was due to the regional administration, in contrast to the i.v. injection. (D) Posterior lung image acquired after intraarterial injection of 99mTc-MAA. Significant tracer accumulation in lung is indicative of tumor shunting. (E) Whole-body image shortly after intraarterial infusion of FU. High FU accumulation in the liver is due to tumor shunting.

flow towards the pelvis and away from normal soft tissue structures (40). Both studies failed to assess tumor accumulation of the cytostatic agent. Studies in our laboratory have demonstrated that FU accumulation increases with blood flow, until optimal flow values are reached. Increasing flow further results in a decreased FU accumulation.

Experimental studies have shown that a correlation between blood flow and glutamate uptake only exists in untreated animals; after irradiation blood flow tends to increase and 13N-glutamate tumor-to-muscle uptake drops (41,42). In our study the accumulation of 13N-glutamate is related to both blood flow and 13N-glutamate extraction.

TABLE 4
Median Values for Perfusion, Shunting, 13N-glutamate, and 18F-FU Uptake

Perfusion	7.5%
Shunt	10.1%
13N-glutamate	11.4%
18F-FU	9.2%

FIGURE 11. A correlation coefficient of 0.80 was obtained for tumor perfusion, ^{13}N-glutamate accumulation, and FU uptake.

Filc-DeRicco et al. performed animal studies with ^{13}N-glutamate in the Walker 256 carcinosarcoma (43). The authors were able to demonstrate that 17.8% of the injected activity was incorporated into aspartate. These results support the dual aspect of tumor glutamate accumulation, which may explain why this parameter was different from ^{99m}Tc-MAA accumulation. The correlation between FU uptake and ^{13}N-glutamate accumulation in the tumor region may indicate that a high FU transport into the cell is associated with increased tumor metabolism. Further studies with metabolically active tracers are required.

The shunt fraction failed to correlate with the FU accumulation. Thus, arterial occlusion may only be useful to reduce blood flow to the optimum level. It should be noted that the shunting fraction was high in all colorectal malignancies, indicating that a reduction of shunting may be advantageous for intraarterial chemotherapy.

The i.v. injection of ^{18}F-FU demonstrated low FU metabolite concentrations in the tumor (Fig. 10), whereas selective administration significantly enhanced the FU accumulation. The relation between tumor and normal soft tissue is significantly higher following intraarterial tracer injection, and therefore less side effects can be expected from intraarterial therapy in this case. Despite regional administration of the cytostatic agent, metabolite concentrations 2 hr after intraarterial tracer injection were only twofold higher compared with the systemic administration of FU. These data show that local delivery of FU can enhance FU metabolite concentrations in the tumor region. The uptake of FU was limited by tumor perfusion and shunting; therefore, only limited palliative effects can be expected from regional administration.

Treatment of Hepatic Metastases and Evaluation with 5-Fluorouracil

Early studies by Yonekura et al. have demonstrated the utility of imaging colonic metastases to liver with [^{18}F] FDG and PET (44). In addition, limited clinical trials now have demonstrated the ability to monitor growth and

regression of these lesions following therapy using FDG by either i.v. or intraarterial administration (45,46).

The standard chemotherapeutic agent for the treatment of hepatic metastases from colorectal cancer is FU (37). The metabolism of FU has been studied extensively and was recently summarized by Hull et al (47). Kinetic data about FU have been obtained from normal tissue as well as tumors in animal experimental studies. Radiolabeled cytostatic agents such as ^{18}F-FU are being used to evaluate therapeutic response. Tissue distribution studies, which analyzed the uptake of ^{18}F-labeled pyrimidines in organs of AH109A tumor-bearing rats, were reported by Abe et al. (48). Shani and Wolf used an animal model to demonstrate that drug-responsive tumors have higher concentration ratios of ^{18}F-labeled FU than drug-resistant tumors (38). While FU concentrations in the blood of human patients undergoing chemotherapy have been reported (47); we have no detailed data on time-dependent concentrations achieved in liver metastases of patients.

Intravenous Chemotherapy

Forty patients with ^{18}F-labeled FU were examined to obtain quantitative data on the time activity pattern of FU and metabolites in metastases. The standard chemotherapeutic protocol included the infusion of FU (500–1500 mg/m^2/24 hr) for 5 days, followed by a 3-wk interval without chemotherapy. To exclude potential effects of chemotherapy on PET results, the patients were examined with PET either preceding the FU therapy (n = 6), or at least 1 wk following the last FU application in the drug-free interval of the therapeutic cycle (n = 34). Liver metastases were diagnosed before referral to the PET examination. Computed tomography (Somatom DRH, Siemens Co., Des Plaines, IL) immediately preceded the PET examination, and was used in each patient to identify the region of greatest metastasis diameter. Only patients who had at least one metastasis identified in two contiguous CT slices (8 mm slice thickness) were included in the study, due to the limited resolution of PET. Fluorine-18-labeled FU (370–444 MBq) was given together with 500 mg unlabeled FU in a short 12-min infusion using an infusion pump. Twelve 2-min images followed by seven 5-min images and six 10-min images were acquired for a total time of 2 hr. The transverse slices were compared to the corresponding CT images to permit secure identification of the mass.
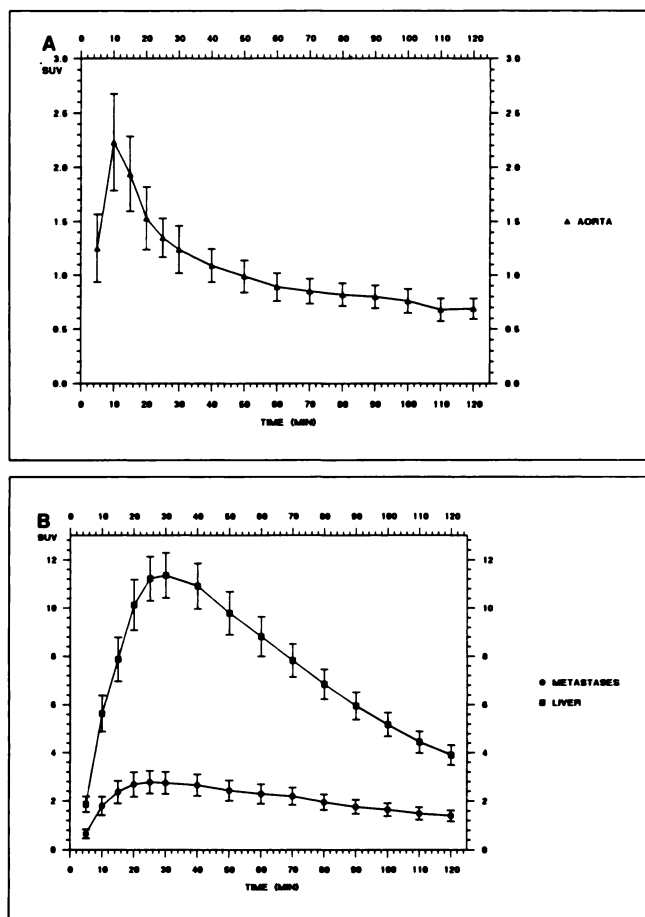
The visual inspection of early PET images may show the metastases in the late phase either as poorly delineated or discrete cold defects against the normal high liver tissue (Fig. 12). The visual inspection proved inadequate for evaluating tracer uptake in metastases when these were viewed against the liver background. In most patients a clear difference in ^{18}F tumor concentrations was not observed when early and late images were compared visually.

The normal liver tissue of 40 patients as well as 65 metastases were evaluated. Furthermore, concentration

FIGURE 12. PET cross section demonstrating low tracer concentrations in liver metastases. High uptake of ^{18}F-labeled FU in the normal liver parenchyma.

values for the aorta were obtained using the ROI technique. Fluorine-18 uptake was expressed as standardized uptake values (SUV). Time-dependent tracer concentrations for the aorta, normal liver parenchyma, and metastases are shown in Figure 13. The highest ^{18}F concentration was noted for the aorta 10 min after the beginning of the 12-min FU infusion (Fig. 2), followed by a rapid decrease when infusion ended. Maximum liver activity after infusion of the cytostatic agent was 11.4 SUV (mean value) with a standard deviation of 1.87 SUV. The time-to-maximum tracer uptake was 30 min (mean value), and

FIGURE 13. (A) Time-activity curves (mean values) for the aorta (n = 40) up to 2 hr after a 12-min FU infusion. (B) Time-activity curves (mean values) for 65 metastases and 40 livers.
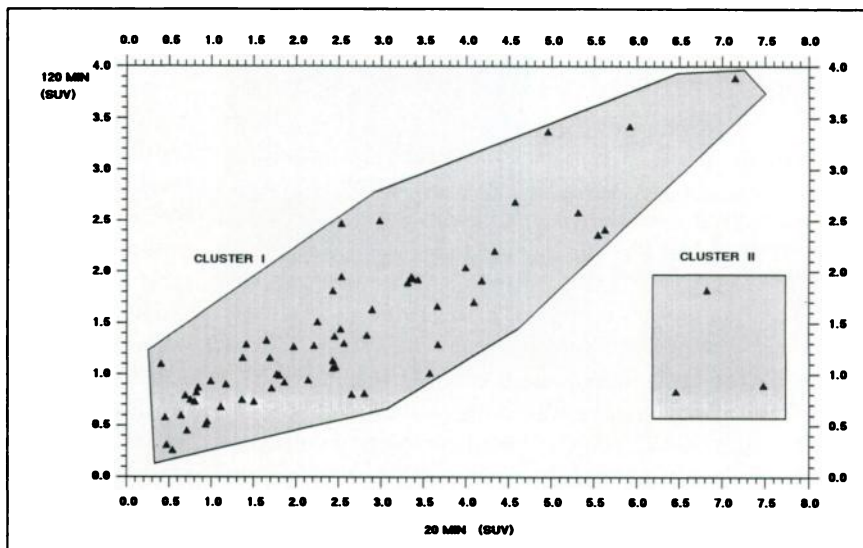
ranged from 25–40 min after infusion. The highest liver-to-aorta ratios were obtained 40–60 min after FU infusion.

The activity of individual metastases was low and relatively constant during the acquisition time after initial distribution phase (Fig. 13). The mean ^{18}F activity in metastases was slightly less than one third of the concentration measured in normal liver parenchyma at 120 min postinjection (Fig. 13). The metastasis-to-aorta ratios ranged from 2–3:1 from 25–120 min after FU infusion.

The PET images taken 8 min after 12-min FU infusion were evaluated to quantify FU transport into the tumor cells, whereas late images, 2 hr after FU injection, were used to estimate the intracellular FU and its metabolically active fraction, since the concentration of free FU in the plasma was low at this time (48). Fluorine-18 incorporation in metastases showed considerable variation, as seen in the differing concentration values (Fig. 14). Cluster analysis (weighted average linkage method with quadratic differences) demonstrated two groups when 20 min and 120 min SUV for metastases were compared (Fig. 14). A linear correlation was obtained for metastases in cluster I (n = 62, r = 0.8821, p < 1%). Regression analysis of 20 min and 120 min SUV in cluster I showed that 120-min ^{18}F concentrations were lower than 20-min values by a factor of 0.44. High FU uptake and low metabolite concentrations were noted only in three metastases, which were identified by cluster II.

Chemotherapy with fluorouracil has been extensively used since its introduction more than three decades ago. Depending on both the selection process and response criteria used, reported response rates have varied from 8% to 82% (37). Based on a literature survey, Kemeny reported that the average response rate for hepatic metastases was 23% (37). With individual response rates low, and population response rates highly variable, it is impossible to predict the response rates of individuals or identify those most likely to respond to therapy. One possible approach for predicting response to FU requires radiolabeling of the chemotherapeutic drug with [18]F. Fluorine-18-FU is biochemically identical with the nonlabeled cytostatic agent FU. Therefore, PET with the ^{18}F-labeled drug gives the oncologist an opportunity to determine tissue concentration of FU and its ^{18}F-labeled metabolites, and to determine their relative tissue concentrations. Since FU uptake by a tumor is prerequisite for successful chemotherapy, the concentration measurements of ^{18}F-FU and metabolites in metastases may help to identify those patients who meet this first criterion of therapeutic success.
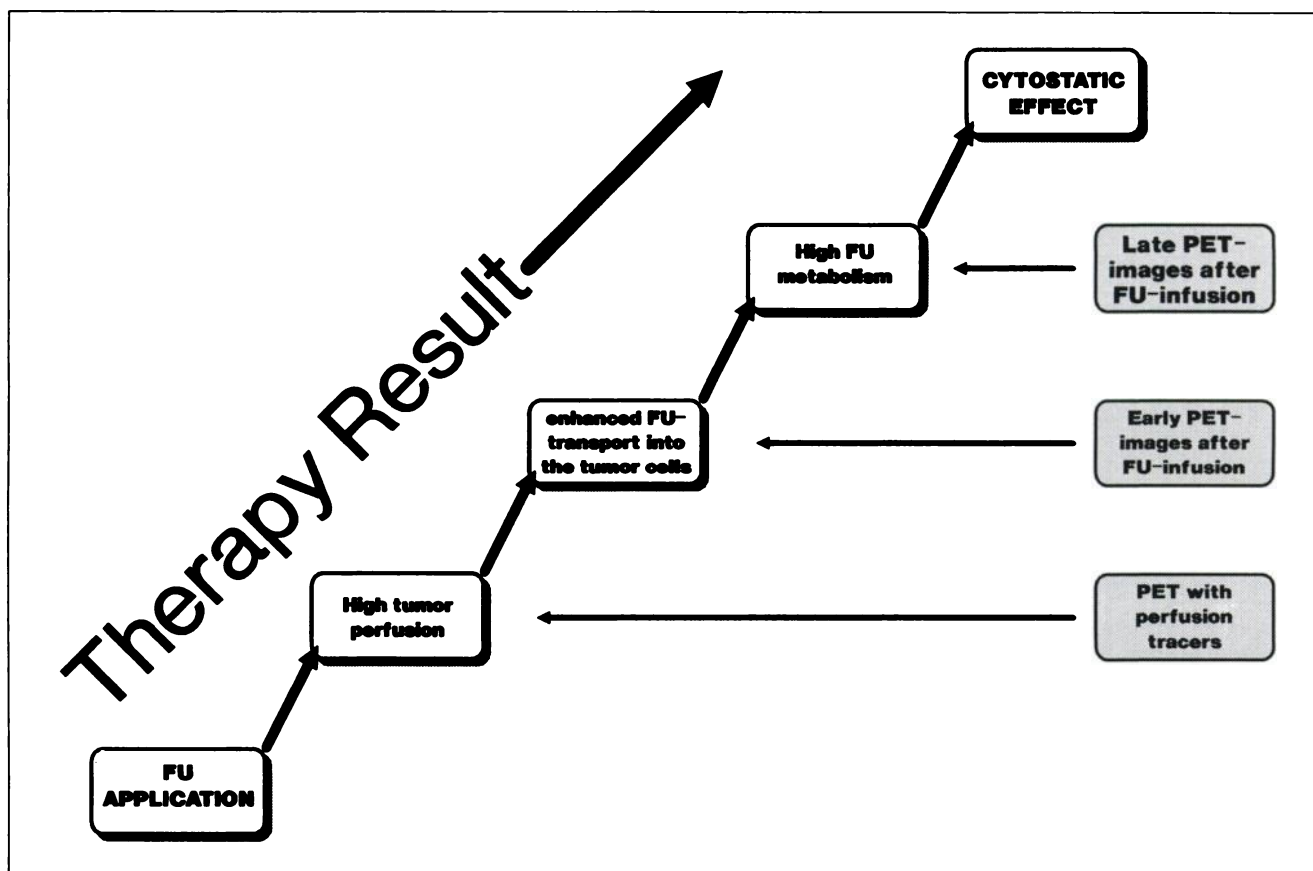
Different steps are required to achieve high FU metabolite concentrations, in order to obtain a good therapeutic result (Fig. 15). Adequate tumor perfusion is required to obtain high FU concentrations in the target area. This step can be measured with PET using a nonmetabolized tracer like ^{15}O-labeled water. While PET with [15]O has been evaluated for brain studies, no experimental data are available for the liver. Angiographic studies in patients with

FIGURE 14. FU uptake and FU metabolism in 65 metastases. Cluster analysis identified two groups. A correlation coefficient of 0.88 was obtained for Group 1.

liver neoplasms have shown that most of the lesions are hypervascular on the hepatic arteriogram (*49*). Furthermore, almost all lesions exhibited some degree of tumor stain. Therefore, most of the metastases may have a good blood supply. Twenty-minute PET images were used in our laboratory to estimate FU uptake in the cells, since the initial decline of the plasma curve for ^{18}F activity is

fast (half-life = 10 min), as reported by Finn et al. (*50*). Furthermore, Young reported that the metabolite fraction in the plasma is < 3% 30 min after FU application (*51*), which suggests rapid intracellular FU transport. Chaudhuri et al. studied the degradative pathway of fluorinated pyrimidines and reported that even 60 min after injection of 25 mg/kg FU in mice bearing sarcoma-180, 61% of the

FIGURE 15. Steps required for a sufficient FU chemotherapy of liver metastases.

radioactivity in the tumor was represented by nonmetabolized FU (52). Wolf et al. observed a trapping of nonmetabolized FU in VX2 tumors with a half-life of 0.4–2.1 hr (53). Therefore, PET images 20 min after FU infusion are adequate to evaluate the nonmetabolized FU in tumor tissue.

Significant differences were found when the early FU uptake and the late ^{18}F concentrations were compared. We were able to demonstrate a linear correlation in 62 of 65 metastases between FU uptake values and FU metabolite concentrations (Fig. 14). These data show that in most patients an increased FU uptake in the tumor should be achieved to obtain high metabolite concentrations. Therefore, regional application or high FU doses should be considered to enhance the cytostatic effect of FU. Conversely, we observed low metabolite concentrations in the presence of high FU uptake in three lesions. This reflects the possible high efflux of FU out of the metastases in some patients, resulting in low FU metabolite concentrations. In these patients, high-dose therapy should have no enhanced effect on therapy outcome. PET with ^{18}F-FU may be used to select those patients prior to chemotherapy.
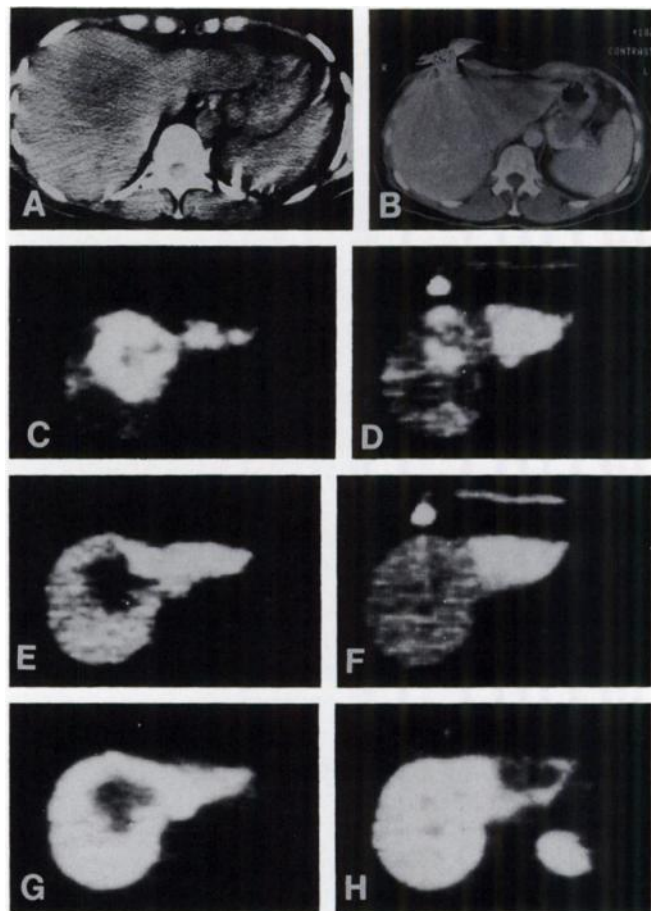
Intraarterial Chemotherapy

The regional administration of fluorouracil has been found to improve selectivity of the cytostatic drug (54). Theoretically, regional delivery can potentially increase drug concentrations at tumor sites and lower systemic drug exposure when compared with systemic drug administration. Patients were examined with ^{18}F-labeled FU and ^{15}O-labeled water to obtain quantitative data about perfusion and FU accumulation. The primary goal was to evaluate tracer concentrations following i.v. and intraarterial infusion of FU. Change in perfusion due to regional application with altered FU accumulation was also evaluated.

Twenty-six examinations of 13 patients were evaluated after i.v. and intraarterial tracer application. All patients had surgically implanted catheters in the gastroduodenal artery. Patients were examined prior to first chemotherapeutic cycle or at least 1 wk following last FU application in the drug-free interval of the chemotherapeutic cycle.

All patients were examined with ^{15}O-labeled water (1110–3700 MBq) prior to FU infusion. Five 1-min images were acquired after i.v. application of ^{15}O-labeled water. A second tracer intraarterial injection was performed 10 min following the first series and again five 1-min images were acquired. Fluorine-18-labeled FU (370–444 MBq) was given together with 500 mg unlabeled FU in a 12-min infusion using an infusion pump following perfusion studies. Sequential images (typically 22 images) were acquired for 2 hr after onset of FU infusion. Intravenous and intraarterial examinations were performed in each patient on different days.

All PET cross sections were generated using an iterative reconstruction program. ROIs were placed over the me-
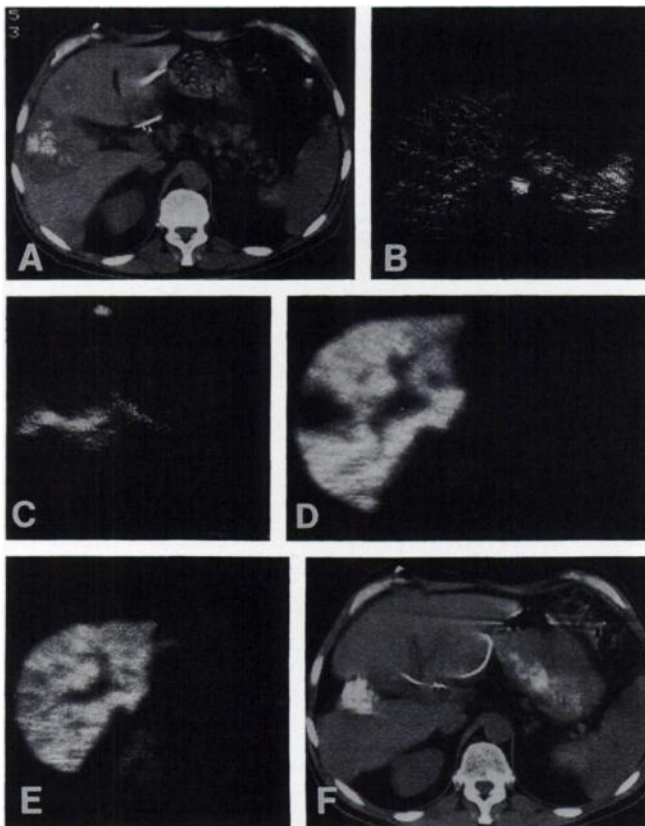
tastases, normal liver parenchyma, and aorta. Time-activity data were calculated from each image series for further evaluation. SUV for ^{15}O-labeled water were calculated from data obtained from the last of the five 1-min scans. The ^{18}F concentration values 2 hr after FU infusion were used to compare the accumulation of the cytostatic agent. Figure 16 demonstrates a PET study in a patient with a doublet-port system (surgically implanted catheters in the gastroduodenal artery and portal vein). The intraarterial application of ^{15}O-labeled water showed a preferential high perfusion of both metastases, while FU transport, as determined by PET images shortly after the end of the infusion, was different for the two lesions. FU metabolite concen-

FIGURE 16. (A) CT cross section of a liver metastasis in the right lobe. (B) CT cross section of a liver metastasis in the left liver lobe of the same patient. Artifacts are due to an intraarterial port system. (C) PET image of the metastasis in the right liver lobe shortly after intraarterial injection of ^{15}O-labeled water. There was preferential perfusion of the lesion. (D) PET image of the metastasis in the left lobe after intraarterial injection of ^{15}O-labeled water. High tracer accumulation was due to the arterial blood supply of the lesion. (E) Low FU transport into the cells shortly after the end of a 12-min infusion. (F) High FU transport into the cells in the metastasis in the left lobe in contrast to the lesion in Figure 16E. (G) Low ^{18}F concentrations 2 hr after tracer injection. (H) In spite of the increased FU transport into the metastasis (Fig. 16F), low ^{18}F concentrations were noted in the images 2 hr after tracer infusion.

trations, obtained from the 2-hr images, were low in both lesions. This example demonstrates that PET can be used to evaluate tumor perfusion, FU transport, and metabolism for different metastases and normal liver parenchyma.

The study in Figure 17 demonstrates a significant enhancement of FU metabolite concentration in the metastasis due to regional application. In contrast to the case in Figure 16, high selective perfusion of the lesion was associated with high FU metabolism. FU transport, as measured in the initial PET images shortly after the end of the FU infusion, was extremely high in both patients. The results show that tumor perfusion and FU transport are separate from FU metabolism. Selective perfusion and increased FU transport are prerequisites for enhanced FU metabolism (Fig. 17). High FU metabolite concentrations lead to tumor regression, as shown by CT follow-up studies (Fig. 17). Since FU uptake in malignancies is a prerequisite for therapy response, regional administration has been

FIGURE 17. (A) CT image of a large, calcified liver metastasis prior to therapy. (B) PET image after i.v. injection of ^{15}O-labeled water. The lesion is seen as a defect. (C) PET cross section after interarterial injection of ^{15}O-labeled water. There was preferential perfusion of the metastasis. (D) PET image 2 hr after i.v. infusion of ^{18}F-labeled FU. Low FU metabolite concentrations were noted in the lesion. (E) PET cross section 2 hr after intraarterial infusion of FU. The tracer concentrations in the metastasis are comparable to the normal liver parenchyma. Significant enhancement of the FU accumulation is due to the regional administration. (F) CT follow-up study 3 mo after intraarterial FU chemotherapy. Significant reduction of the tumor volume was due to the preferential accumulation of FU in the lesion.

used to enhance the drug exposure of the tumor. The primary goal is to extend some partial responses to complete responses and some minimal responses to at least partial responses (37,55). We were able to investigate both systemic and regional infusion of FU in 13 patients. The double examinations with perfusion tracer ^{15}O-labeled water demonstrate that regional injection improves access to the lesions of 13 of 15 metastases, whereas the ^{18}F-FU metabolite concentrations were enhanced in only 9 metastases. These results show that a high tumor perfusion is not the only prerequisite for increased FU uptake in metastatic lesions. FU transport into tumor cells, demonstrated by the PET images acquired shortly after the end of FU infusion, may be different from the perfusion as shown in our patient study (Fig. 16). Furthermore, even a high FU transport into the cells is not necessarily followed by a high FU metabolism (obtained from PET images 2 hr after FU infusion). We would like to emphasize that successful chemotherapy therefore requires preferential perfusion of a mass, high FU transport into the tumor cells, and increased metabolism of FU. Since only some patients profit from this approach, individual measurements of tumor perfusion, FU transport, and metabolism are required to evaluate the possible advantage of regional chemotherapy.

Fluorouracil Accumulation and Therapeutic Results

The estimation of FU chemotherapy outcome prior to therapy is one of the unsolved problems in oncology. Hull et al. found no significant difference in metabolite concentrations in plasma between responders and nonresponders to FU chemotherapy (47). They state that detection of FU metabolites in tumor tissue is required for an assessment of response to FU. Shani and Wolf showed in an animal study that high metabolite concentrations are required for a good therapeutic result (38). These data indicate that FU metabolite measurements in tumor tissue may be helpful to predict response to FU chemotherapy in patients.

Patients were examined prior to the first chemotherapeutic cycle with ^{18}F-labeled FU and PET to obtain quantitative data about FU and metabolites in metastases. CT studies were performed before and after FU chemotherapy and tumor volume was calculated from the cross-sections. FU metabolite concentrations obtained from PET images prior to chemotherapy were compared with the tumor growth rate during chemotherapy. Our primary goal was to determine the correlation between these parameters to predict therapeutic outcome on the basis of PET studies.

Eighteen metastases obtained from 12 patients with liver metastases from colorectal carcinoma were evaluated. Standard therapeutic protocol includes i.v. or intraarterial infusion of FU (500–1500 mg/m^2/24 hr) for 5 days, followed by a 3-wk interval without chemotherapy. To exclude potential effects of chemotherapy on PET results, patients were examined with PET prior to their first FU therapy cycle.

Liver metastases were diagnosed prior to referral to PET. Computed tomography immediately preceded PET examination, and was used in each patient to identify the region of greatest metastasis diameter. The volume of each metastasis examined with PET was calculated from CT cross-sections using a three-axis method (Volume = (4/3) π a b c). CT studies preceded the first chemotherapeutic cycle and were repeated 3–11 mo later. Growth rate was obtained from volumetric data using the formula growth rate = ln(Vol2/Vol1)/(days between CT studies), in which Vol1: volume of metastasis before chemotherapy and Vol2: volume of metastasis after chemotherapy. The doubling time of a lesion was calculated from the growth rate by doubling time = ln(2)/growth rate. Visual inspection of the late PET image showed the metastasis as a defect (Fig. 18), which is indicative of low FU metabolism. FU uptake in the normal liver tissue was high compared with the metastasis. The SUV were 1.91 for the metastasis and 4.06 for the liver parenchyma. The doubling time was 91 days for the lesion. This case shows that without a high FU metabolism no decrease in tumor volume can be expected. High FU metabolite concentrations can result in therapeutic success as demonstrated in Figure 16. We obtained a significant correlation coefficient (r = 0.86) for the tumor growth rate and the 2-hr FU metabolite concentrations (Fig. 19).
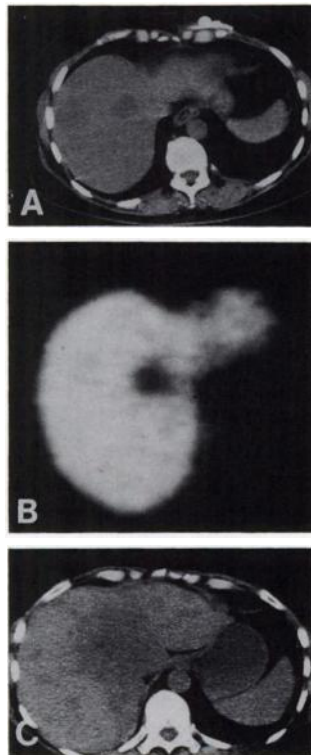
The SUV represent concentration values normalized for injected dose and body volume. Whereas SUV of 1 represents a homogenous distribution of injected activity, accumulation of radiolabeled tracer results in elevated SUV numbers. We noted only 4 of 18 metastases with

FIGURE 18. (A) CT section demonstrating a liver metastasis in the cranial part of the right liver lobe. Examination prior to FU therapy. (B) Low FU accumulation in the metastasis prior to chemotherapy, indicative for low probability of response. (C) CT follow-up study 4 mo after FU chemotherapy, showing significantly increased tumor volume, but no response to therapy.

SUVs exceeding 3.5 (Fig. 19). Late images obtained 2 hr after FU infusion represent total FU metabolite concentrations. It should be remembered that some FU metabolites, such as 9-fluoro-beta-alanine, show no significant antitumor activity. Therefore, measured ^{18}F concentrations may fail to mirror the cytotoxic potency of FU metabolites. It follows that tracer uptake alone, as measured by PET, may not be predictive for therapeutic success, but therapeutic success cannot occur without uptake of the cytostatic agent. When low metabolite concentration values are measured in tumor tissue, planned or initiated chemotherapy has a low probability of success. When high ^{18}F concentrations are noted in the tumor, the patient should have a high probability of response. While tumor regression occurred only at SUV exceeding 3.5, no tumor regression was noted for lower concentration values (Fig. 19). The data show that PET with FU can be used to estimate therapy outcome. The noninvasive, quantitative evaluation of FU accumulation in metastases enables the oncologist to optimize and individualize FU chemotherapy.
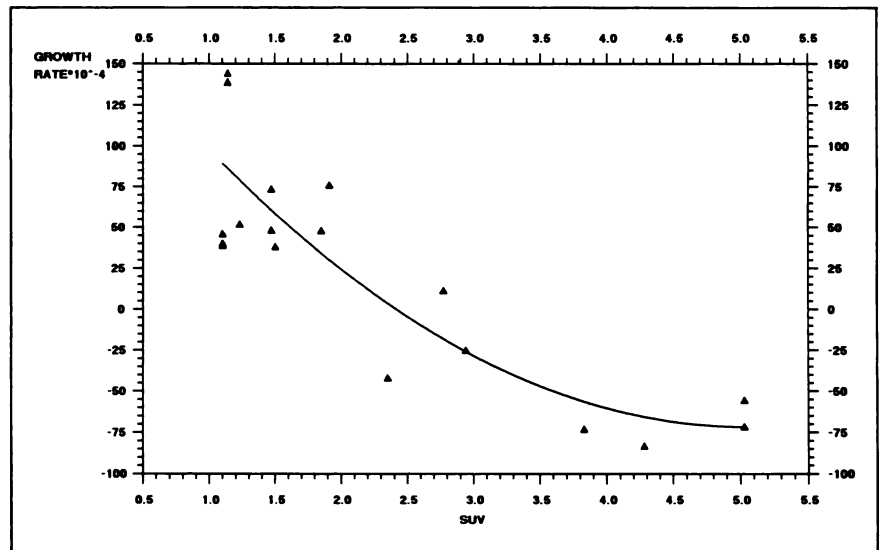
ORO- AND HYPOPHARYNX CARCINOMAS

Systemic chemotherapy of advanced cancer of the head and neck is applied either in combination with radiation therapy and/or surgery or as a single measure. Combinations of FU and cisplatinum have proven useful with remission rates between 50% and 80% (56). Ultrasound, computed tomography (CT), and magnetic resonance tomography provide mainly morphologic data. This is achieved by interpreting parameters like echogenicity or attenuation, proton density, or relaxation times. In contrast, PET with FDG is a specific method that delivers functional information about glucose metabolism. We evaluated the effect of chemotherapy on tumor metabolism in patients with PET.

Ten male patients with histologically proven tumors of the oro- or hypopharynx (9 squamous-cell carcinoma, 1 anaplastic carcinoma) underwent a PET examination before and after the first chemotherapeutic cycle with cisplatinum (150 mg/m^2 on Day 1) and FU (1000 mg/m^2 on Days 1–4). Only patients with a tumor or lymph node diameter exceeding 1.5 cm were accepted. Eight-mm-thick continuous sections were acquired in CT. Tumor or lymph node volumes were calculated from CT images using a region-of-interest technique. The function c = ln(V$_0$/V$_1$)/(t$_1$-t$_0$) with V$_0$ and V$_1$ as the volume before and after therapy and t$_0$ and t$_1$ as the time for V$_0$ and V$_1$ was used for calculation of tumor growth rate. PET examinations were performed with a two-ring detector system and three PET sections with a thickness of 11 mm were acquired. FDG was used to assess regional glucose uptake and phosphorylation. One hour after i.v. administration of 333–444 MBq (9 to 12 mCi) FDG, PET images were acquired for 10 min and cross-sections were generated by use of an iterative reconstruction program. Spatial resolution was

FIGURE 19. FU accumulation and tumor growth rate in 18 lesions (12 patients). A correlation coefficient of 0.86 was observed for both parameters.

5.1 mm with a pixel size of 2 mm. Attenuation and scatter correction were done. For quantitative evaluation, ROI were defined in tumor and soft tissue. Identification of anatomic structures was done by comparing PET sections with CT images. FDG uptake was then expressed as the SUV. FDG data were available for five tumors and nine lymph nodes. Volumetric data existed for four tumors and seven lymph nodes. Regional FDG metabolism and changes after therapy are demonstrated in Figure 20. Different lymph nodes may show a different FDG uptake pattern even in the same patient. The relation between the change in FDG uptake and the growth rate is shown in Figure 21. The data demonstrate that the same change in FDG metabolism results in a higher reduction in tumor volume compared with lymph node volume.

A second group of 27 patients with hypopharynx carcinomas were studied with PET and FDG prior to surgery. During surgery tumor specimens from the target area evaluated with PET were obtained and one-dimensional
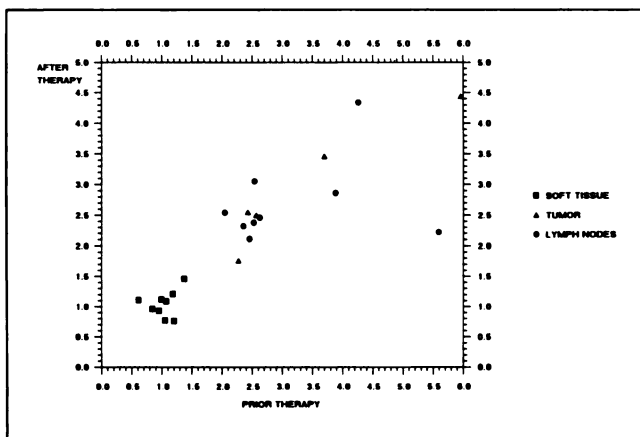
flow cytometry was used to determine the proliferative index:

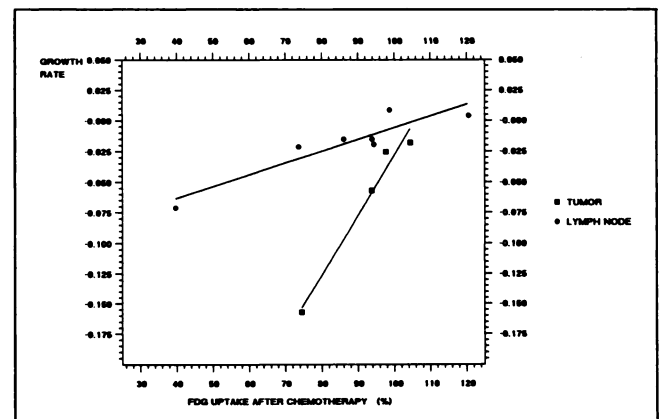$$PI = 100 * (S + G2 + M) / (G0/1 + S + G2 + M).$$

PET FDG data were compared to the histologic grading of the tumor as well as the flow cytometric data.

Comparison of FDG uptake in the tumor area and histologic grade of the lesion revealed no evidence for a correlation. The relation between FDG accumulation and the proliferative index is demonstrated in Figure 22. Two groups with a high (>3.5 SUV) and low (<3.5 SUV) FDG uptake are shown. We noted a significant correlation between the two parameters for both groups (Figs. 23 and 24). There was no correlation between tumor perfusion as measured by ^{15}O-labeled water and the proliferative index.
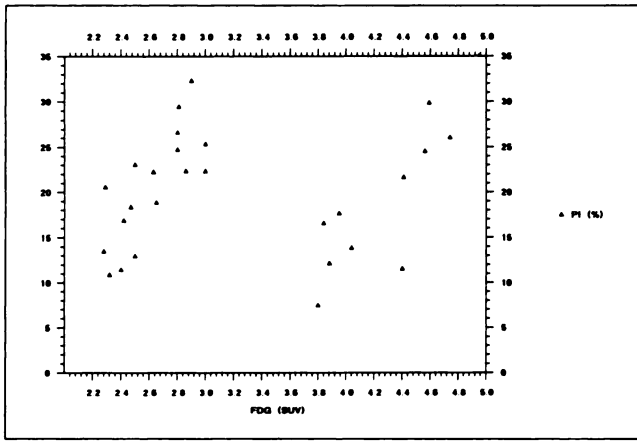
The assessment of tumor metabolism in patients undergoing therapy is important for the evaluation and individual planning of therapy regimens. Gallium scanning has been used in conventional nuclear medicine for treatment control. In a tumor model a dependence of

FIGURE 20. FDG uptake prior to and after chemotherapy in tumors (n = 5), lymph nodes (n = 9) and in normal soft tissue (n = 9).
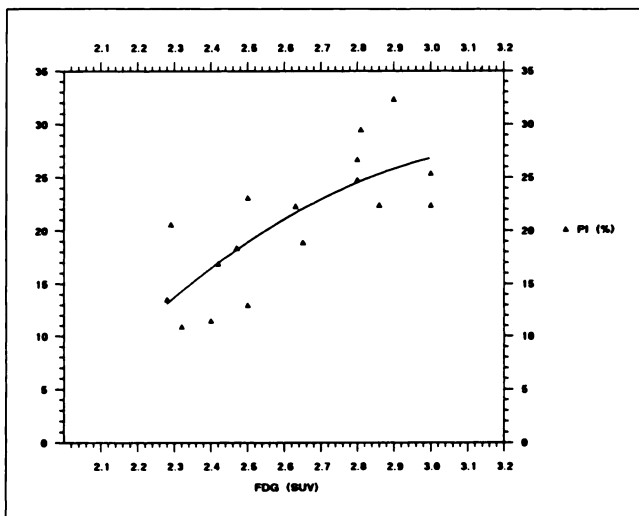

FIGURE 21. FDG uptake after therapy (percent of uptake prior to therapy), and growth rate of the lesions (4 tumors, 7 lymph nodes).
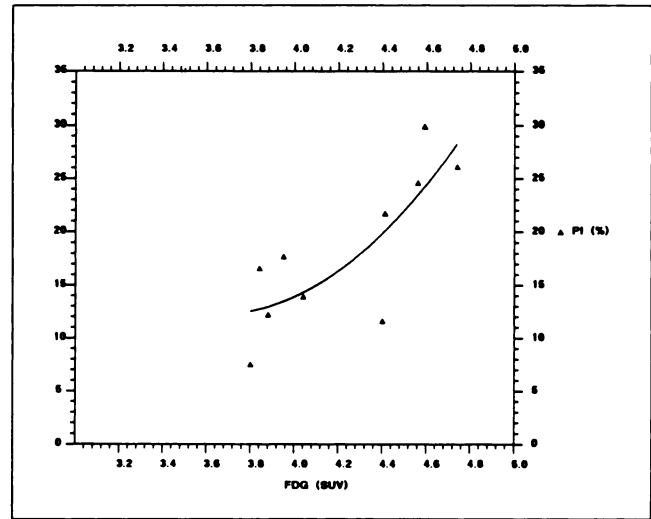
FIGURE 22. FDG uptake prior to therapy and proliferative index. Two groups with a high and low FDG uptake were observed.

Gallium uptake on the amount of viable cells was observed (57). Bichel et al. found that a high incorporation of Gallium corresponded to a high proliferation rate (57). However, the exact mechanism of Gallium uptake in the cell is not yet known. The incorporation of a transferrin-Gallium-complex is controversial (59). FDG as an analog of glucose is transported like glucose into the cell, then phosphorylated and trapped as FDG-6-phosphate, since there is no significant further metabolism of FDG-6-phosphate. This accumulation in metabolic active cells can be used for differential diagnosis in patients with probable recurrent colorectal cancer (7). A further application of the PET-FDG method is the evaluation of treatment response measuring glucose metabolism before and during therapy. Clinical and experimental studies report a decreasing FDG uptake in tumors treated with radiation therapy (60). In our ongoing study, we found that FDG

FIGURE 23. A correlation coefficient of 0.76 was obtained for the FDG uptake and the proliferative index when lesions of FDG uptake values below 3.5 were evaluated.

FIGURE 24. A correlation of 0.80 between the FDG uptake and the proliferative index for lesions with FDG values exceeding 3.5 was noted.

uptake prior to chemotherapy was increased in all tumors and lymph nodes. In most cases, we observed uniform changes in FDG accumulation during therapy. However, a difference in degree was found. Lymph nodes in the same patient can show differences in metabolic activity before and during therapy. This indicates the heterogeneity of the tumor cell population.

We found a linear relation between changes in metabolism and growth rate with different regression functions for tumors and lymph nodes. Six tumors or lymph nodes had no significant change in tumor metabolism. In a flow cytometric study by Brauneis et al. (61) no significant difference was found in response to therapy in tumors with different proliferation rates. However, there was a higher incidence of regional or distant metastases in tumors exhibiting a high proliferation rate. Ploidity and proliferating activity are widely accepted as markers for the biologic behavior of malignant tumors. Watanabe et al. performed a study with rat brain tumors and found a significant correlation between malignancy as measured by the bromodeoxyuridine labeling index and the local cerebral glucose utilization, whereas no correlation was noted for tumor blood-flow (62). They suggested that increase in glucose utilization in these tumors is required for nucleic acid synthesis. Minn et al. observed a high correlation of FDG uptake and the amount of S-phase-cells (63). This supports the hypothesis that FDG reflects proliferative activity and incidence of metastatic spread. In contrast to Minn et al., we noted two groups with a different regression function for the proliferative index (Figs. 23 and 24). At present, the interpretation of these data is mainly speculative. One possible explanation may be the expression of an oncogene, which enhances glucose transport. Experimental data have shown that the expression of the ras-oncogene increases the uptake of deoxyglu-

cose (64,65). Therefore, the presence of oncogene in tumor tissue is being measured in ongoing studies.

FDG uptake must be seen as an in vivo measure for the aggressiveness of a tumor. Using PET, it is possible to gain absolute and comparable data about tumor metabolism before and after chemotherapy. PET is a useful method for observation and improvement of clinical therapeutic protocols in patients undergoing systemic chemotherapy.

LUNG TUMORS

The diagnostic work-up of patients with lung tumors remains a difficult clinical challenge even with the use of many imaging methods. The evaluation of bronchogenic carcinoma by current imaging techniques such as plain-film, CT, and MRI is mainly limited to morphologic information. Several groups compared the staging of bronchogenic carcinoma by CT or MRI with surgical staging and report a sensitivity of 25–71% for lymph nodes and 52–80% for the primary tumor (66,67).

These results are still quite unsatisfactory and thus new, noninvasive methods with improved staging accuracy are required. The morphologic information obtained by conventional imaging methods may be expanded by PET with FDG to assess bronchogenic carcinoma with a metabolically active compound (68–70). Since malignant tumors show increased metabolic activity, FDG accumulates in those lesions. This uptake can be used in PET studies to visualize the tumor with high contrast to the surrounding tissue and to quantify the tracer uptake as a measure of its metabolic activity (71–73). Fuijiwara et al. found a possible correlation between uptake of ^{11}C-methionine and tumor histology in squamous-cell carcinoma and large-cell carcinoma (11). The goal of our study was to evaluate FDG uptake in lung tumors prior to therapy and compare tracer uptake with histology of the masses. Furthermore, T-staging with conventional methods was compared with PET with reference to surgical staging.

All studies were performed as end point studies with emission scan started at 50 min postinjection. Fluorine-18-labeled FDG (440 MBq) was used for these studies to localize the most relevant cross-sections to be studied for PET and to obtain a TNM-staging. CT scans of the thorax were performed in each patient immediately prior to PET. Contrast material was injected when required. Reference points were marked for positioning the patient in the PET-scanner. PET cross-sections were compared with corresponding CT scans as well as PET transmission images in order to clearly identify areas of tracer uptake. ROIs were placed on desired areas to allow quantitative evaluation of uptake distribution in the PET images. Tracer uptake was expressed as the SUV.

Tumor Metabolism Prior to Therapy

We evaluated 100 patients with completed clinical staging for suspected bronchogenic carcinoma before therapy with PET and F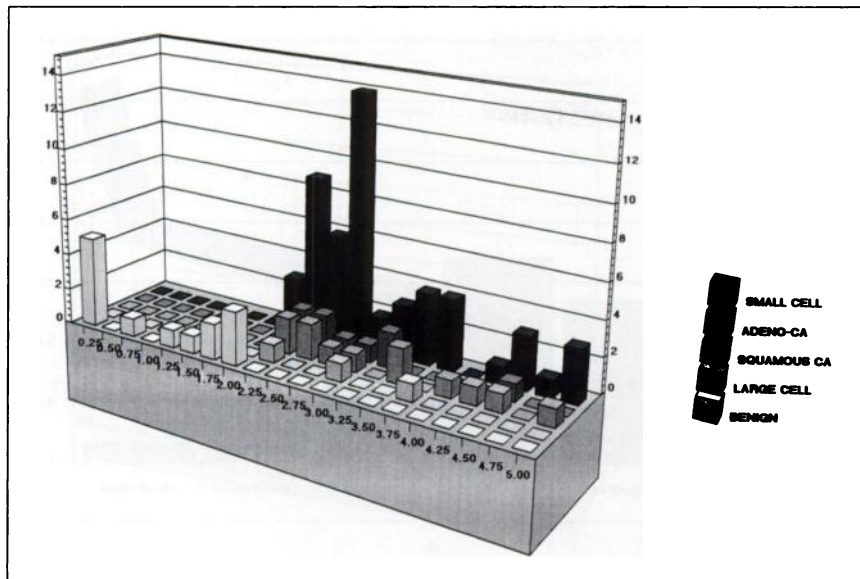DG to determine metabolic activity of the lesions. Double-tracer studies with ^{15}O-labeled water and FDG were performed to compare tumor blood-flow and metabolism. Whereas 13 patients had benign lesions (hematoma, inflammation, tuberculosis), a malignant tumor was found in 87 patients. FDG uptake values in relation to histology of the masses are shown in Figure 25. No differences in SUV were observed for tumors with different histology. Data on FDG uptake and correlation to tumor histology are not reported in the literature for a large number of primary lung tumors. Fuijiwara et al. performed PET studies with ^{11}C-methionine in 16 lung tumors with 4 different histologies and found a significantly different tracer uptake for squamous-cell carcinomas (n = 9) and large-cell carcinomas (n = 5), whereas no correlation to small-cell carcinoma (n = 1) and adenocarcinoma (n = 1) could be evaluated due to the limited number of cases (11). In contrast, we noted no statistically significant difference in FDG uptake and tumor histology (Fig. 25). Furthermore, evaluation of tumor blood-flow with O-15-labeled water showed no correlation to FDG uptake (Fig. 26). Malignant and benign lesions showed a significantly different FDG uptake (Fig. 27). We noted an overlap of the SUV between malignant tumor and tuberculosis in 3 cases (Fig. 27). Kubota et al. also found accumulation of ^{11}C-methionine and FDG in aspergilloma and abscesses, which did not permit differentiation from tumor (70).

Tumor Staging

Surgical resection was performed in 20 patients with a malignant tumor after conventional TNM-staging and T-staging with PET. In 8 of the 20 malignant tumors, PET correctly changed the T-classification compared with the conventional staging, while in 12 cases no differences were noted. PET was able to differentiate benign from malignant tissue, whereas CT failed to demonstrate morphologic differences (Figs. 28 and 29). These data demonstrate that PET will play a major role in the staging of bronchogenic carcinoma. Further studies are required to evaluate the potential of PET for the N-staging. Due to the limited range of our system the lymph nodes could not be evaluated sufficiently.

Changes in Tumor Metabolism Due to Therapy

Evaluation of the success of chemotherapy is one of the problems in primary lung tumors. We performed follow-up PET studies in patients with small-cell carcinomas to evaluate early changes in tumor metabolism and to compare these data with the change in tumor volume as measured by CT (71,74,75). The effect of chemotherapy (Endoxan, Doxorubicin, Etoposid) and/or radiotherapy was evaluated in 18 patients. Each patient was studied prior to therapy with subsequent follow-up studies beginning after the second chemotherapeutic cycle, or one-third of the planned total radiation dose. Fourteen of the 18 patients received chemotherapy, 1 patient was directed to radiotherapy, and 3 patients underwent a combined treatment protocol. Restaging was performed 3 mo after onset

FIGURE 25. While benign and malignant lesions were differentiated with high accuracy using FDG uptake values, no differences were found for tumors with different histologies.

of therapy and change in FDG uptake was compared with final clinical evaluation as well as change in tumor volume.

The FDG uptake as quantified by SUV data decreased in all 12 patients responding to the given therapy. Of those 12 patients, 4 (33%) did not show a decrease in volume and were falsely considered nonresponders by plain-film x-ray since the tumor volume did not change. Of those six patients not benefiting from therapy, four (67%) showed a decrease in tumor volume that was falsely presumed to be a sign of response to therapy, whereas FDG uptake remained constant or increased. FDG-PET identified 4 patients as responders who were falsely regarded as nonresponders and 4 patients as nonresponders who were regarded as responders, thus changing the evaluation in 8 of 18 patients. In the assessment of therapy response over a complete treatment cycle, Figure 30 shows the changes of FDG uptake of a patient receiving primary radiotherapy of an unresectable adenocarcinoma. The initial PET study

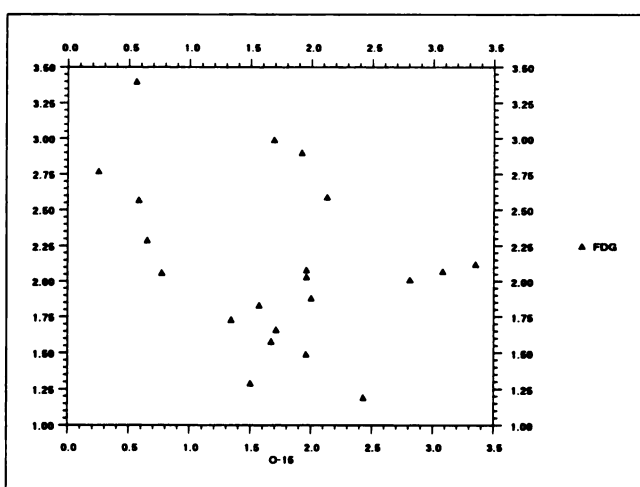**FIGURE 26.** No correlation was found for the tumor perfusion and metabolism.

was on Sept. 27, 1989 with SUV of 4.3. After a 40-Gy dose, an initial follow-up PET study on Oct. 10, 1989 showed a decrease in SUV to 2.7. In a restaging study after completion of therapy, a follow-up on Jan. 31, 1990 showed a continued decrease in SUV to 2.2. Following this restaging, the patient received additional endoluminal radiotherapy of 4.5 Gy as a boost. The last follow-up on Apr. 24, 1990 showed a continued decrease in SUV to 1.91. This uptake was significantly lower than the value prior to therapy, but was still increased compared with normal tissue. Based on this residual intense metabolism, the patient was referred to a thoracic surgeon and admitted for surgery. Surgery and histologic specimens showed that the area of increased FDG uptake was a region of residual tumor growth.

Mesotheliomas do show high tumor-metabolism prior to therapy (Fig. 31). Seven follow-up studies were made up to 827 days after onset of therapy in a patient with a large mesothelioma (Fig. 32). The patient received intra-tumoral injections of interleukine. Quantitative evaluation of FDG uptake demonstrated short-term regression due to therapy and then slow tumor progression. PET proved valuable in this patient by directing the therapy to those areas most metabolically active (Fig. 32). Whereas no differences were noted in conventional x-ray and CT, PET was able to demonstrate a patchy FDG uptake pattern in the solid masses.
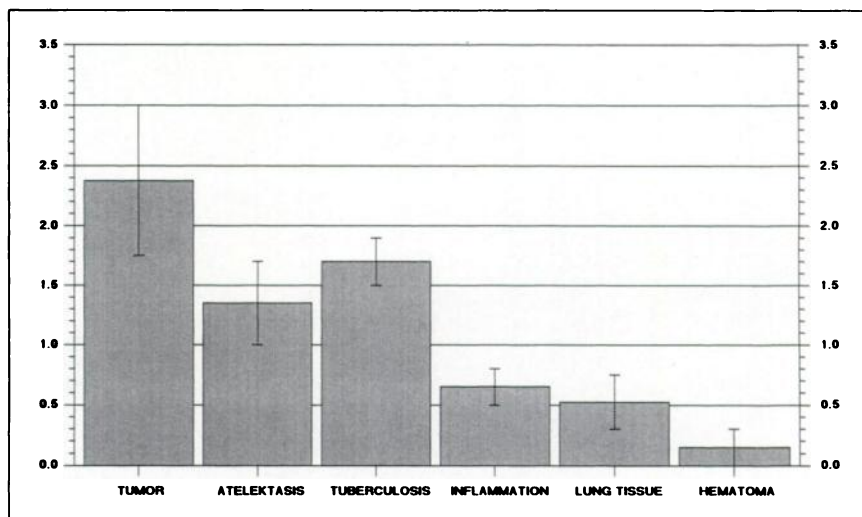
When we evaluated changes in FDG uptake and changes in tumor volumes, three different patterns were noted:

1. A decrease in tumor volume and FDG uptake.
2. An increase in tumor volume and FDG uptake.
3. An initial decrease in tumor volume, followed by an increase later on, while FDG uptake was constant.

In most of our patients an increase or decrease in tumor volume was preceded by a corresponding change in FDG

FIGURE 27. Mean and standard deviation for different benign and malignant lesions.
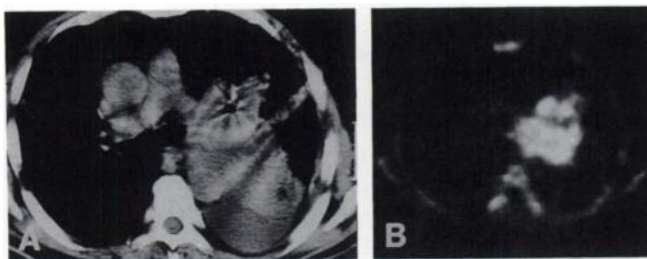
uptake. These data are comparable to short-term FDG follow-up data and restaging data obtained 3 mo after therapy. Therefore, PET measurement of FDG uptake is a more reliable and sensitive method to evaluate therapy outcome than change in tumor volume. The most important finding was the third pattern (Fig. 33). Since small-cell carcinomas have some cell lines that are resistant to a cytostatic agent whereas other cell lines are susceptible, the initial decrease in tumor volume is misleading. The constant, high FDG uptake in these tumors in the presence of a decrease in tumor volume may be indicative of an increasing selection of resistant cell lines in the tumor. PET is capable of making this distinction and may be used to recommend changes in therapeutic approach.
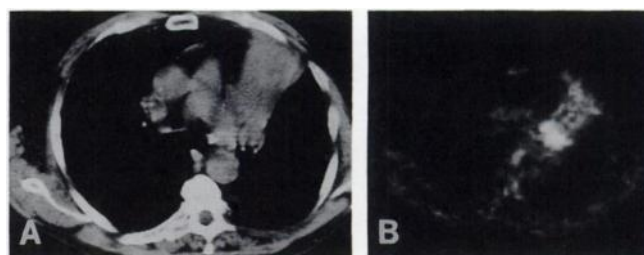
PRIMARY AND METASTATIC BRAIN TUMORS

PET has provided new insights into the evaluation of primary and metastatic intracranial tumors. Fluorine-18-FDG is currently the principal radiotracer used for tumor grading and determination of prognosis in primary brain tumors (3,76–80). It has also been used to help distinguish the presence of recurrent tumor from radiation changes secondary to therapy (81–83). Evaluation of metastatic

intracranial cancers is also possible in the clinical setting, as demonstrated in Figure 34. These images demonstrate elevated FDG accumulation in a metastatic melanoma located in the temporal lobe of a patient previously treated with radiation therapy, chemotherapy, and hyperthermia. Catheters used to deliver intracranial chemotherapy have been removed but their prior location can be visualized as contrast-enhancing tracts leading to the tumor mass on T1-weighted MRI images following administration of gadolinium. In this case, the clinical question was whether the tumor had spread from the known lower enhancing mass upward along the tracts. FDG accumulation was seen only in the region of the mass in the temporal lobe suggesting the presence of active tumor glucose metabolism. No activity was observed along the tracts leading to the brain surface. In fact, the low levels of FDG activity observed as a wedge-shaped area of surrounding brain correlated with prior radiation ports from previous treatment with external beam radiotherapy.
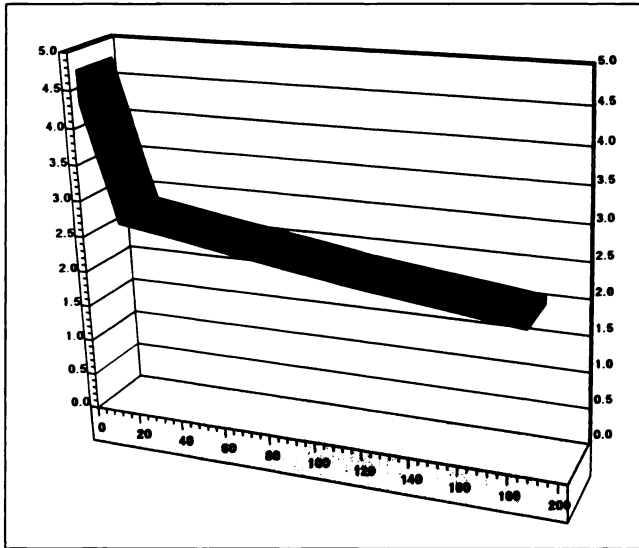
While FDG has provided useful information about brain tumor growth, grading, and prognosis, the technique is not without problems. Investigators have reported variability in the rates of glucose utilization within tumors of similar pathologic grades (80), suggesting that a direct correlation of glucose utilization with the degree of tumor

FIGURE 28. (A) CT image of a tumor near the left hilar region. The tumor tissue could not be differentiated from the surrounding atelectasis. (B) The PET image 1 hr after FDG injection shows the metabolically active tumor. Low tracer accumulation seen in atelectasis.

FIGURE 29. (A) Left central tumor with atelectasis of the upper lobe. (B) the PET image demonstrates increased tumor metabolism and an elevated FDG uptake in the atelectasis due to poststenotic inflammation.

FIGURE 30. PET follow-up studies in a patient with adenocarcinoma treated with radiation therapy. Decreasing tumor metabolism in response to therapy and remaining abnormal metabolism even after additional therapy were noted.

FIGURE 32. (A) Conventional image of a mesothelioma of the right lung. (B) CT image of the tumor in the right upper lobe. Soft-tissue masses were noted in the peripheral and mediastinal part of the lung. (C) The PET FDG image shows that the peripheral mass does have a high metabolism. Therapy could be focused on this lesion.
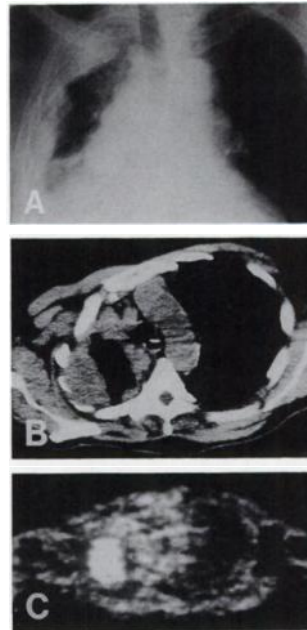
malignancy as measured by histological grade may not always hold.

While variation in patient populations, such as previously-treated versus untreated tumors, may account for such findings, other possible explanations may exist. For example, the metabolic requirements of the tumor may vary according to the overall nutritional status of the patient regardless of the fasting state or the presence of other systemic disorders that may be present in conditions such as diabetes or sepsis. It is also possible that metabolic rates are linked to oncogene expression and the density of glucose transporter proteins (64,65). In addition, elevated or decreased FDG can potentially be seen in other conditions frequently included in the differential diagnosis of intracranial mass lesions or simultaneously occurring with tumor such as infection, inflammation, seizure activity, radiation necrosis, edema, and infarct (70,84,85). Mineura et al., for example, note the increased accumulation of FDG in tumor and other entities, such as cerebral sarcoidosis and abscess, and suggest that other tracers such as ^{15}O-water be used for further metabolic analysis designed to differentiate such lesions (84).

Several investigators have found ^{11}C-labeled methionine to be superior to ^{11}C-deoxy-D-glucose or FDG for deline-
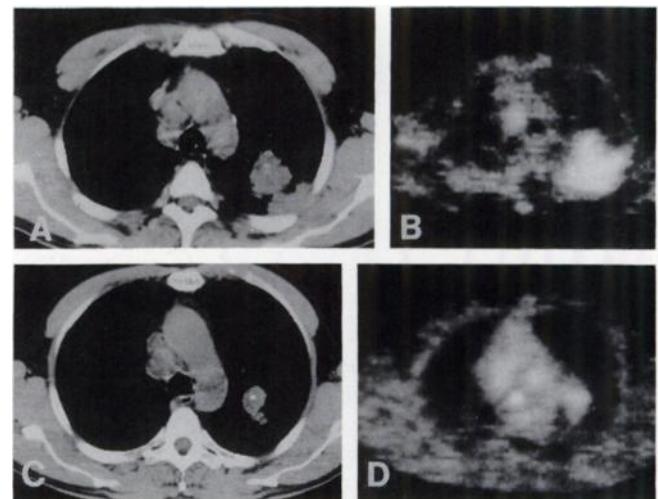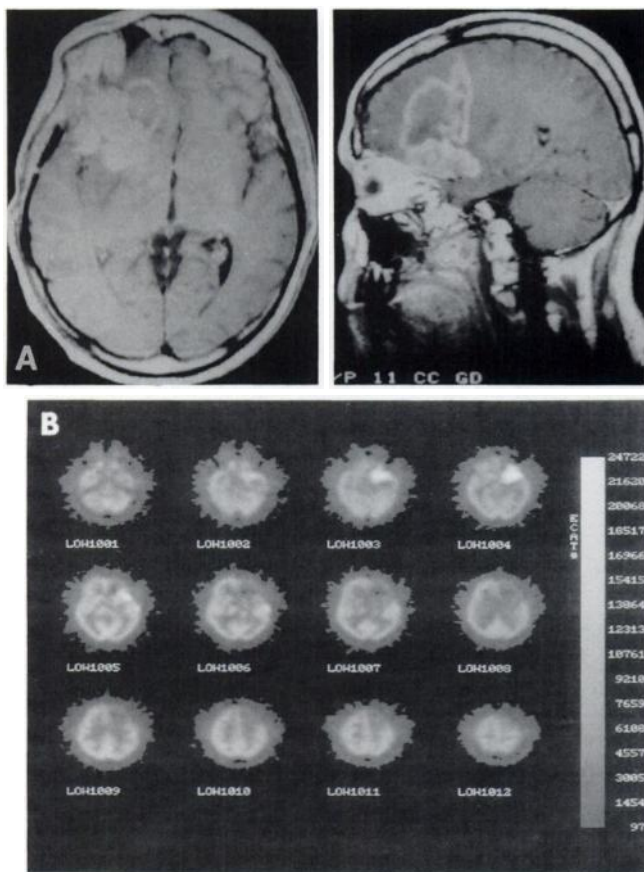
ation of tumor margins and for differential diagnosis of tumor recurrence from radiation necrosis (85–87).

Accumulation of ^{11}C-methionine and FDG into intracranial lesions has been evaluated for recurrent tumor and six cases of radiation necrosis (70). The data suggest that FDG be used initially to determine the presence of hypermetabolism in the lesion. If such a lesion were hypermetabolic compared with normal brain, radiation necrosis could be ruled out. However, a hypometabolic lesion would require a follow-up study with ^{11}C-methionine, with

FIGURE 33. (A) CT image of a small-cell carcinoma with mediastinal lymph node metastases prior to chemotherapy. (B) The PET FDG image shows the increased metabolism in the malignant lesions. (C) Significantly decreased tumor volume after chemotherapy. (D) The PET FDG study gives evidence of an unaltered tumor metabolism, which is indicative for the selection of resistant cells during therapy. This study was followed by tumor progression in the next 4 wk.

FIGURE 31. High tumor metabolism in a mesothelioma of the right lung.

FIGURE 34. (A) Gadolinium enhanced MR images transaxial and sagittal through intracranial metastatic melanoma. (B) PET FDG cross-sectional study from skull base through vertex. Marked uptake of FDG was observed in tumor mass in right temporal parietal zone. Figure 34A is (reprinted with permission from *Cancer*.)

FIGURE 35. (A) T1- (left) and T2- (right) weighted MR images of mass lesion in the right frontal lobe. No enhancement with gadolinium was observed. (B) PET FDG shows low accumulation of activity in lesion relative to normal brain. (C) Carbon-11-methionine uptake observed in same lesion. (D) Blocking of ¹¹C-methionine uptake by orally administered phenylalanine.

accumulation of ¹¹C activity being higher in low-grade (hypometabolic) lesion compared with necrosis.

While more direct comparative studies are required, it should be noted that information obtained from each radiotracer is complementary and that together such information may be more useful than individual tracer data alone. Figure 35 shows the most recent scans in an ongoing case of an unknown mass lesion in a patient who presented with seizures. Repetitive FDG and ¹¹C-methionine studies have shown consistent findings over a 1-yr period. The lesion is seen as a nonenhancing low-density lesion on T1-weighted MRI with little mass effect. High focal signal intensity is seen on spin density images. FDG images demonstrate a well-defined area of low-tracer accumulation compatible with a low-grade tumor. A ¹¹C-methionine scan demonstrates moderate tracer accumulation in the lesion. Blockade of ¹¹C-methionine uptake with phenylalanine (100 mg/kg p.o. 60 min prior to second study), which competes with methionine for cellular transport, demonstrates decreased accumulation of ¹¹C-methionine in both normal brain and the mass lesion. Moderate tracer
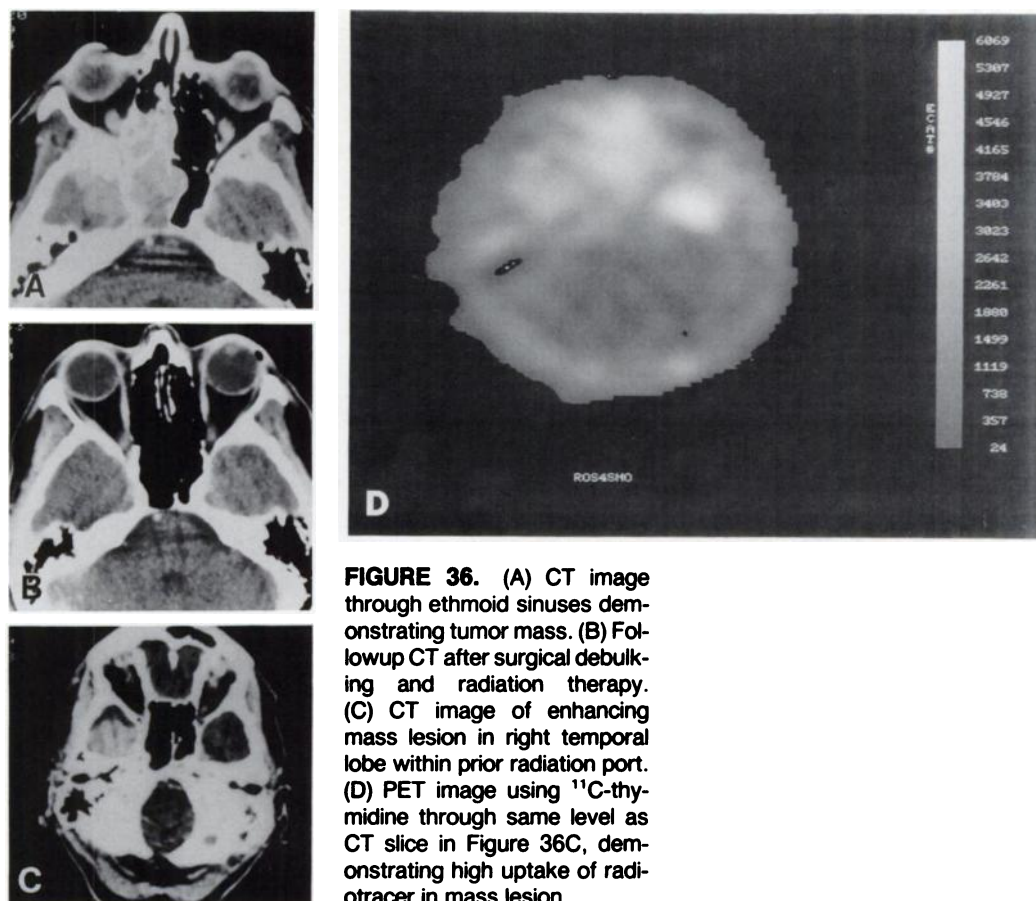
accumulation suggests the presence of a low-grade lesion, since larger amounts of ^{11}C-methionine uptake are usually observed in high-grade lesions. In addition, effective blockade of amino acid uptake into the lesion demonstrates the presence of viable tissue. While the presence of a low-grade lesion can be inferred from the FDG study, other entities such as infarct cannot be ruled out. Additional useful information, therefore, has been obtained from the methionine study, which demonstrates active metabolism in viable tissue. Thus, the studies provide useful complementary information. Final diagnosis has yet to be made by biopsy, but follow-up studies will continue as there exists the possibility of malignant degeneration in a low-grade lesion.

Other amino acids are beginning to be used in the evaluation of tumor metabolism in patients, as data from experimental studies have demonstrated the presence of altered amino acid transport and protein synthesis in malignant cells (89-92). Both natural and synthetic amino acids are being studied in patients with brain tumors (86, 93-97). While the measurement of protein synthesis in tumors with radiolabeled natural amino acids such as ^{11}C-methionine may provide specific biologic information on tumor behavior, data is now available suggesting that amino acid transport rather than protein synthesis rates may be more strongly correlated to tumor grade (98). If this is true, then further studies with transport-specific

nonmetabolized amino acids may be warranted (99,100). On the other hand, monitoring alterations in amino acid metabolism appears to be an effective way to evaluate therapy, as exemplified in studies using bromocriptine to treat pituitary adenomas (94,101,102).

On the horizon, newer agents are becoming available that will provide more specific information concerning brain tumor growth characteristics. One example is ^{11}C-putrescine, which serves as a radiotracer of polyamine synthesis (103). The latter synthetic pathway activity is known to be elevated in many tumor types and coupled to cellular replication. Limited clinical trials have demonstrated a correlation between uptake and tumor malignancy (103). Other interesting agents that can potentially bind to receptor sites in primary and metastatic brain tumors are being developed (104).

Finally, ^{11}C-thymidine, which potentially will be the most direct tracer of cellular replication, is currently available for clinical trials (105). The uptake of ^{11}C-thymidine into the intracranial tumors of the five patients studied thus far, including three with high-grade (III-IV) glioma and two with metastatic cancer to brain (small-cell of the ethmoid sinus and adenocarcinoma of the esophagus), has been demonstrated (106). In Figure 36, an example of using ^{11}C-thymidine in a patient suspected of having metastatic cancer is shown. The patient originally presented with an ethmoid sinus small-cell carcinoma that was re-

FIGURE 36. (A) CT image through ethmoid sinuses demonstrating tumor mass. (B) Followup CT after surgical debulking and radiation therapy. (C) CT image of enhancing mass lesion in right temporal lobe within prior radiation port. (D) PET image using ^{11}C-thymidine through same level as CT slice in Figure 36C, demonstrating high uptake of radiotracer in mass lesion.

sected. The patient was subsequently treated with radiation therapy and did well until 1 yr later when she presented with headaches. A contrast-enhancing lesion was found by CT in the lower temporal lobe. Unfortunately, since this solitary lesion was located in the prior radiation port, the differential diagnosis of radiation necrosis versus recurrent tumor was entertained. A PET scan using ^{11}C-thymidine demonstrated focal accumulation of tracer in the lesion bed, compatible with the presence of tumor as opposed to radiation necrosis. Subsequent surgical resection and histological analysis demonstrated metastatic malignant tissue.

While FDG remains the most widely used radiotracer for brain tumor evaluation, several of the above-mentioned agents will probably be used with increasing frequency in the clinical setting as experimental studies prove their efficacy.

LYMPHOMA

Fluorine-18-labeled deoxyglucose has been shown to be a useful agent for imaging both Hodgkin's and non-Hodgkin's lymphoma (107–111). There is evidence to suggest that FDG may be more sensitive than ^{67}Ga-citrate for detecting active disease (107–110). In the study by Paul, results were obtained using a conventional gamma camera with thick lead collimation (107). It is possible that PET scans will provide even greater sensitivity. As in the case of lung cancers discussed above, changes in glucose concentration may not correlate with volume changes noted with CT. Yoshikawa et al. demonstrated that in 7 lymphoma patients, changes in glucose metabolism were greater than volume changes noted on CT examination following radiotherapy, suggesting that response to therapy may be detected earlier than using conventional imaging techniques (109). In 14 patients with non-Hodgkins lymphoma, 3 with high-grade, 5 with intermediate-grade, and 6 with low-grade lesions, higher uptake was observed with ^{11}C-methionine compared with FDG (111). Low-grade lesions, importantly, were not visible using FDG.

Recent developments in imaging lymphoma have also occurred using ^{11}C-thymidine. In one study, investigators demonstrated uptake of ^{11}C-thymidine into lymphomas in a series of 10 patients (112). The patient population included low-, intermediate-, and high-grade lesions with tumors varying in size and located in different anatomical sites. Using a limited mathematical modeling scheme and partial corrections for the presence of radiolabeled metabolites, the investigators were able to obtain estimates of thymidine phosphorylation rates that correlated with histologic grade. Other investigators have noted changes in ^{11}C-thymidine uptake into lymphomas following therapy, and have shown this agent to be useful in distinguishing fibrosis from active tumor (112).

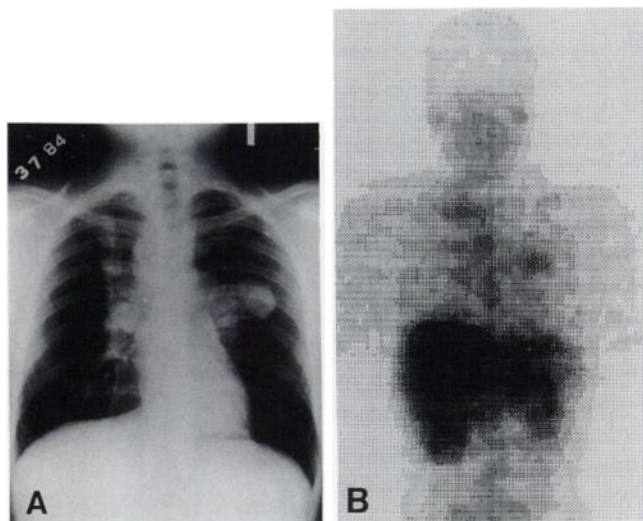More detailed studies with larger patient populations are required, including pre- and post-therapy trials to further evaluate the potential of PET imaging of lymphoma.

MELANOMA

While there are only a limited number of cases demonstrating the utility of PET for imaging malignant melanoma, the most commonly used tracers are ^{11}C-labeled alpha-amnioisobutyric acid (AIB) and FDG (114–116). Both agents have been used to image metastatic melanoma in the body, but only FDG has been used in intracranial lesions (115).

Investigators at the Sloan-Kettering Institute have imaged several patients with malignant melanoma in various anatomical sites using ^{11}C-AIB and a high-energy rectilinear device for total-body scanning (114,117). In Figure 37, a chest x-ray demonstrates large metastatic mass lesions in the perihilar and mediastinal zones. A scan of the patient's chest demonstrates increased radiotracer in regions corresponding to the tumor masses. Normal low lung, heart, and soft-tissue activity provide good target-to-background ratios. Note the absence of intracranial activity compatible with the known inability of AIB to cross the intact blood-brain barrier due to the absence of A types or alanine-preferring transport system on the capillary endothelial cell membrane required for AIB entrance into the brain. Lesions of varying size located in other anatomical sites including the extremities, abdomen, and pelvis have also been successfully imaged due to the general low, normal levels of background activity (117). Further studies using PET are necessary to evaluate the full potential of this agent for imaging metastatic melanoma.

FDG has been used to image lesions in patients with metastatic melanoma undergoing a variety of therapy protocols (116). Preliminary results have demonstrated that

FIGURE 37. (A) Chest radiograph of patient with metastatic malignant melanoma in lung and mediastinum. (B) Rectilinear scan of chest in same patient demonstrating uptake of ^{11}C-AIB in tumor lesions. (Figure 37B is reprinted with permission from Ref. 114.)

BREAST CANCER

Investigators of primary and metastatic breast cancer have focused on the use of ^{18}F-FDG and estrogen derivatives for imaging with PET. FDG has been used to successfully image patients with primary breast cancers prior to and following completion of combination chemohormonotherapy (118–120). Following administration of FDG (10 mCi), tumor uptake was measured at 50–60 min postinjection. Reduction in tumor/normal breast uptake ratios occurred within 8 days of therapy without significant reduction in tumor size determined by mammography. Subsequent tumor shrinkage was generally noted by the third cycle of therapy (21 days/cycle). The results suggest that FDG can be used to assess early response to therapy for breast cancer prior to changes in tumor morphology. Metastatic breast cancer to bone, lymph nodes, liver, and the mediastinum has also been successfully imaged with FDG (45,120).

Other investigators have developed tracers that are being evaluated for the imaging of estrogen and progestin receptors on breast tumor cells. PET imaging of estrogen receptors using ^{18}F-labeled 16-alpha-fluoroestradiol-17β has been accomplished in primary breast cancers as well as in axillary nodal metastatic disease (121,122). A good correlation (r = 0.96) has been observed between the uptake of the ^{18}F-estradiol derivative in primary tumors with estrogen receptor concentrations measured using in vitro techniques following tumor excision. This technique has promise as a method by which quantitative receptor analysis can be performed using noninvasive techniques prior to therapy with antiestrogens. PET offers the capability of making such measurements throughout the entire lesion as well as metastatic foci without the need for multiple biopsies, and can potentially be used to evaluate antiestrogen therapy response (121).

Imaging of progestin receptors in the desired setting has been less successful thus far. A progesterone analog, 21-[^{18}F]-fluoro-16-alpha-ethyl-19-norprogesterone, which demonstrated potential for imaging progestin receptors in an animal model, showed low-target tissue uptake in a small number of human subjects (123).

Although few in number, the preliminary clinical imaging studies in patients with breast cancer suggest that multiple radiotracers measuring different biochemical processes may be used to provide useful information for tumor evaluation. The determination of which agents or combination of agents will be most efficacious must await further study.

BONE AND SOFT-TISSUE TUMORS

Soft-tissue tumors were among the first cancers to be evaluated using metabolically active PET radiotracers. Ni-trogen-13-labeled glutamate, for example, prepared by an enzymatic synthesis (124), was used to image patients with osteogenic sarcoma and Ewing's sarcoma (125–127). An osteogenic sarcoma in a 9-yr-old patient was successfully imaged with ^{13}N-glutamate prior to chemotherapy. A 40% decrease in tumor uptake was observed following completion of 10-wk therapy protocol correlated with return of an elevated serum alkaline phosphatase to a normal value (125). In a follow-up study, 10 patients with osteogenic sarcoma were treated with preoperative adjuvant chemotherapy (127). Regions of interest (2 cm × 2 cm) from scans obtained before and after completion of therapy were compared with thin-section histological specimens obtained at surgery. Decreased uptake of ^{13}N activity (> 30%) corresponded to areas of necrotic tumor, whereas regions of increasing accumulated activity were observed in areas of high residual cell viability.

In the case of Ewing's sarcoma, all 11 patients with primary disease were successfully imaged prior to therapy (126). Scans obtained with ^{13}N-glutamate demonstrated a more marked change in radioactivity accumulation compared with ^{99m}Tc-MDP following chemotherapy. The changes observed in ^{13}N-glutamate accumulation in lesions appeared to correlate with clinical and histologic response to therapy. This agent, however, was unable to detect metastatic disease in the lungs or bone, although various biologic and technical factors may have accounted for such findings, including the use of rectilinear scanning versus PET cross-sectional imaging.

Carbon-11-labeled AIB has been evaluated in patients with malignant fibrous histiocytoma, demonstrating high target-to-background ratios in extremity lesions (128). These preliminary clinical trials followed the demonstration that this agent could be used to image sarcomas in spontaneous canine tumor models (129).

Musculoskeletal tumors have more recently been imaged with PET techniques using ^{18}F-FDG (130–132). Preliminary imaging studies have demonstrated a correlation between glucose utilization rate and tumor grade, although the number of patients studied was small (130). In addition, quantification of glucose utilization rates in soft-tissue tumors is only an approximation since values for the lumped constant and kinetic rate constants are not known (130). A semiquantitative approach using the DUR normalization to patient weight and dose method was used by Griffith et al. to evaluate FDG uptake in 14 patients with soft-tissue masses (131) and compared with a simple ratio of tumor/normal tissue evaluation method. No overlap was observed between malignant and benign soft-tissue masses when the DUR method was applied, but in eight cases overlap was observed in the simple ratio method. In another series, however, both the tumor-to-background ratio and dose-adjusted ratio (normalized to patient weight and dose) techniques produced statistically significant differences between benign and malignant tissues (132). Further investigations are necessary to determine the appro-

priate analytical methodology as well as the choice of radiopharmaceuticals used.

CONCLUSION

The current applications of PET in the study of neoplasms of the body is limited compared with brain studies. One of the main reasons for this is the lack of a large number of whole-body PET systems. Another fundamental issue has been the relative lack of interest in PET applications in tumors of the body. It is becoming clear, however, that as the number of PET centers with whole-body units increases, more interest will be generated in somatic cancers. The results from investigators currently working in the field thus far demonstrate that PET will play a major role in the diagnosis and treatment of a variety of cancer patients. The key question for the clinical application of PET is the gain in information by PET over morphologic methods like ultrasound, CT, and MRI. Further PET studies are required to evaluate the full potential of PET in relation to conventional imaging. Whatever the future role of PET in oncology, the modality should be evaluated not in comparison with morphological imaging, but as a means of providing additional physiological information that can be correlated with anatomy. More information needs to be known about the metabolism of PET radiopharmaceuticals in tumors. Additional in vivo experimental studies are needed to evaluate such metabolism. The interpretation of such metabolic studies should not be limited, however, to a pure qualitative or semi-quantitative evaluation of tumor metabolism, but should be expanded to explore parameters such as tumor growth rate, metastatic potential, and oncogene expression. The future for PET applications in oncology will be bright when it is possible to evaluate in vivo the fundamental processes of tumor growth and response to therapy using this noninvasive methodology.

ACKNOWLEDGMENTS

REFERENCES

1. Wagner HN Jr and Conti PS. Advances in medical imaging for cancer diagnosis and treatment. Cancer 1991;67:1121–1128.
2. Mathias CJ, Welch MJ, Raichle ME, et al. Evaluation of a potential generator-produced PET tracer for cerebral perfusion imaging: single-pass cerebral extraction measurements and imaging with radiolabeled Cu-PTSM. J Nucl Med 1990;31:351–359.
3. Di Chiro G, Oldfield E, Bairamian D, et al. In vivo glucose utilization of tumors of the brain stem and spinal cord. In: Greitz T, Ingvar DH, Widen L, eds. Positron emission tomography. New York: Raven Press, 1985:351–361.
4. Fukuda H, Matsuzawa T, Abe Y, et al. Experimental study for cancer diagnosis with positron-labeled fluorinated glucose analogs: [18F]-2-fluoro-2-deoxy-D-mannose: a new tracer for cancer detection. Eur J Nucl Med 1982;7:294–297.
5. Nagata Y, Yamamoto K, Hiraoka M, et al. Monitoring liver tumor

therapy with [18F]FDG positron emission tomography. J Comput Assist Tomogr 1990;14:370–374.
6. Conti PS, Bading JR, Wong DF, et al. Positron emitting radiotracers: potential aids in the diagnosis and management of neoplasms. Tumor Diagnostik & Therapie 1988;9:175.
7. Strauss LG, Clorius JH, Schlag P, et al. Recurrence of colorectal tumors: PET evaluation. Radiology 1989;170:329–332.
8. Kubota K, Matsuzawa T, Fujiwara T, et al. Differential diagnosis of solitary pulmonary nodules with positron emission tomography using [11C]-L-methionine. J Comput Assist Tomogr 1988;12:794–796.
9. Kubota K, Yamada K, Fukuda H, et al. Tumor detection with carbon-11-labeled amino acids. Eur J Nucl Med 1984;9:136–140.
10. Hatazawa J, Ishiwata K, Itoh M, et al. Quantitative evaluation of L-[Methyl-C-11]methionine uptake in tumor using positron emission tomography. J Nucl Med 1989;30:1809–1813.
11. Fujiwara T, Matsuzawa T, Kubota K, et al. Relationship between histologic type of primary lung cancer and carbon-11-L-methionine uptake with positron emisson tomography. J Nucl Med 1989;30:33–37.
12. Martiat P, Ferrant A, Labar D, et al. In vivo measurement of carbon-11-thymidine uptake in non-Hodgkin's lymphoma using positron emission tomography. J Nucl Med 1988;29:1633–1637.
13. Bolster JM, Vaalburg W, Paans AM, et al. Carbon-11-labeled tyrosine to study tumor metabolism by positron emission tomography (PET). Eur J Nucl Med 1986;12:321–324.
14. Ishiwata K, Ido T, Abe Y, et al. Studies on 18F-labeled pyrimidines III. Biochemical investigation of 18F-labeled pyrimidines and comparison with 3H-deoxythymidine in tumor-bearing rats and mice. Eur J Nucl Med 1985;10:39–44.
15. Dimitrakopoulou A, Strauss LG, Haberkorn U, et al. PET examinations with F-18-labeled fluorouracil in patients with liver metastases from colorectal carcinomas. Eur J Nucl Med 16:S190.
16. Ginos JZ, Cooper AJL, Dhawan V, et al. [13N]cisplatin PET to assess pharmacokinetics of intra-arterial versus intravenous chemotherapy for malignant brain tumors. J Nucl Med 1987;28:1844–1852.
17. Diksic MA, Mitsuka S, Conway T, et al. Use of PET to evaluate in vivo pharmacokinetics of chemotherapeutic agents, BCNU and SarCNU in humans. Tumor Diagnostik & Therapie 1988;9:171.
18. Woodard HQ, Gigler RE, Freed B, and Russ G. Expression of tissue isotope distribution. J Nucl Med 1975;16:958–959.
19. Engenhart R, Kimmig B, Marin-Grez M, et al. Combined neutron-photon-therapy of locally recurrent rectosigmoid tumors. Strahlenther Onkol 1989;165:327–329.
20. Grabbe E, Winkler R. Local recurrence after sphincter-saving resection for rectal and rectosigmoid carcinoma: value of various diagnostic methods. Radiology 1985;155:305–310.
21. Johnson RJ, Jenkins JPR, Isherwood I, et al. Quantitative magnetic resonance imaging in rectal carcinoma. Br J Radiol 1987;60:761–764.
22. Bischof-Delaloye A, Delaloye B, Buchegger F, et al. Clinical value of immunoscintigraphy in colorectal carcinoma patients: a prospective study. J Nucl Med 1989;30:1646–1656.
23. Schmidlin P, Kübler WK, Doll J, et al. Image processing in whole-body positron emission tomography. In: Schmidt HAE, Csernay L, eds. Nuklearmedizin. Stuttgart, Germany: Schattauer; 1987:84–87.
24. Gallagher BM, Fowler JS, Gutterson NI, et al. Metabolic trapping as a principle of radiopharmaceutical design: some factors responsible for the biodistribution of [18F]2-deoxy-2-fluoro-D-glucose. J Nucl Med 1978;19:1154–1161.
25. Som P, Atkins HL, Bandoypadhyay D, et al. A fluorinated glucose analog, 2-fluoro-2-deoxy-D-glucose (F-18): nontoxic tracer for rapid tumor detection. J Nucl Med 1980;21:670–675.
26. Goodman MM, Elmaleh DR, Merk L, et al. F-18-2- and 3-fluorodeoxy-D-glucose as potential diagnostic tracers for tumors [Abstract]. J Nucl Med 1981;21:P37.
27. Paul R, Johansson R, Kellokumpu-Lethinen PL, et al. Tumor localization with 18F-2-fluoro-2-deoxy-D-glucose: comparative autoradiography, glucose-6-phosphatase histochemistry, and histology of renally implanted sarcoma of the rat. Res Exp Med 1985;185:87–94.
28. Als C, Schoutens A, Taton G, et al. SPECT antiCEA immunoscintigraphy (IS) and 18F-FDG PET in the evaluation of colorectal carcinoma. Eur J Nucl Med 1990;16:410.
29. Fukuda H, Matsuzawa T, Ito M, et al. Experimental and clinical study of cancer diagnosis with F-18-FDG using positron emission tomography. J Nucl Med 1984;25:P50.
30. Allum WH, Mack P, Priestman TJ, et al. Radiotherapy for pain relief in locally recurrent colorectal cancer. Ann R Coll Surg Engl 1987;69:220–

221.

31. Beart RW, Martin JK, Gunderson LL. Management of recurrent rectal cancer. *Mayo Clin Proc* 1986;61:448–450.

32. Herzog J, Schmidt B, Fassbender T, et al. Die Stellung der Strahlentherapie in der Behandlung von Lokalrezidiven bei Rektumkarzinomen. *Strahlenther Onkol* 1988;164:121–128.

33. Strauss LG, Heim M, Jaschke W, et al. Intraarterielle Chemotherapie' von kolorektalen Tumoren und Rezidiven. *Tumor Diagnostik & Therapie* 1986;7:225–230.

34. Ogawa T, Shishido F, Inugami A, et al. Assessmemt on changes of blood flow and metabolism in patients with cerebral gliomas following radiochemotherapy. In: Matsuzawa T, ed. *Proceedings of the international symposium on current and future aspects of cancer diagnosis with positron emission tomography.* Sendai, Japan: Tohuku University, 1985;69–74.

35. Davey P, Arnott SJ, Sturgeon CM. Carcinoembryonic antigen as a prognostic indicator in the radiotherapeutic management of rectal cancer. *Eur J Surg Oncol* 1987;13:17–20.

36. Kimball P, Brattain MG. Isolation of a cellular subpopulation from a human colonic carcinoma cell line. *Cancer Res* 1980;40:1574–1579.

37. Kemeny N. The systemic chemotherapy of hepatic metastases. *Semin Oncol* 1983;10:148–158.

38. Shani J, Wolf W. A model for prediction of chemotherapy response to 5-fluorouracil based on the differential distribution of 5-[18F]Fluorouracil in sensitive versus resistant lymphocytic leukemia in mice. *Cancer Res* 1977;37:2306–2308.

39. Wile AG, Stemmer EA, Andrews PA, et al. Pharmacokinetics of 5-fluorouracil during hyperthermic pelvic isolation-perfusion. *J Clin Oncol* 1985;3:849–852.

40. Woods D, Bechtel W, Charnsangavej C, et al. Gluteal artery occlusion: intra-arterial chemotherapy of pelvic neoplasms. *Radiology* 1985;155:341–343.

41. Knapp WH, Helus F, Sinn HJ, et al. N-13-L-glutamate uptake in malignancy: its relationship to blood flow. *J Nucl Med* 1984;25:989–997.

42. Knapp WH, Helus F, Layer K, et al. Nitrogen-13-glutamate uptake and perfusion in Walker 256 carcinosarcoma before and after single-dose irradiation. *J Nucl Med* 1986;27:1604–1610.

43. Filc-DeRicco S, Gelbard AS, Cooper AJL, et al. Short-term metabolic fate of L-[13N]glutamate in the Walker 256 carcinosarcoma. *Cancer Res* 1990;50:4839–4844.

44. Yonekura Y, Benua RS, Brill AB, et al. Increased accumulation of 2-deoxy-2[F-18]fluoro-D-glucose in liver metastases from colon carcinoma. *J Nucl Med* 1982;23:1133–1137.

45. Kim EE, Chung S-K, Tilbury R, et al. Differentiation of residual or recurrent tumors from post-treatment changes with PET using F-18-FDG. *J Nucl Med* 1990;31:803.

46. Schiepers C, Hawkins RA, Hoh C, et al. Total-body imaging with fluorodeoxyglucose (FDG) and PET in patients with malignancies. *J Nucl Med* 1990;31:803.

47. Hull WE, Port RE, Herrmann R, et al. Metabolites of 5-fluorouracil in plasma and urine, as monitored by 19F nuclear magnetic resonance spectroscopy, for patients receiving chemotherapy with or without methotrexate pretreatment. *Cancer Res* 1988;48:1680–1688.

48. Abe Y, Fukuda H, Ishiwata K, et al. Studies on 18F-labeled-pyrimidines. Tumor uptakes of 18F-5-fluorouracil, 18F-5-fluorouridine, and 18F-fluorodeoxyuridine in animals. *Eur J Nucl Med* 1983;8:258–261.

49. Chuang VP. Hepatic tumor angiography: a subject review. *Radiology* 1983;148:633–639.

50. Finn C, Sadee W. Determination of 5-fluorouracil (NSC-19893) plasma levels in rats and man by isotope dilution-mass fragmentography. *Cancer Chemother Rep* 1975;59:279–286.

51. Young D, Vine E, Ghanbarpour A, et al. Metabolic and distribution studies with radiolabeled 5-fluorouracil. *J Nucl Med* 1982;21:1–7.

52. Chaudhuri NK, Mukherjee KL, Heidelberger C. Studies on fluorinated pyrimidines VII—the degradative pathway. *Biochem Pharmacology* 1959;1:328–341.

53. Wolf W, Presant CA, Servis KL, et al. Tumor trapping of 5-fluorouracil: in vivo 19F NMR spectroscopic pharmacokinetics in tumor-bearing humans and rabbits. *Proc Natl Acad Sci USA* 1990;87:492–496.

54. Collins JM. Pharmacologic rationale for regional drug delivery. *J Clin Oncol* 1984;2:498–504.

55. Dimitrakopoulou A, Frohmüller S, Strauss LG, et al. Positron emission tomography (PET) provides an individualized regional tumor therapy in patients with colorectal liver metastases. In: Hammelmann H, ed. *Chirurgisches Forum 1989 für experimentelle und klinische Forschung.* Heidelberg: Springer-Verlag; 1989;497–502.

56. Ervin TJ, Clark JR, Weichselbaum RR. Multidisciplinary treatment of advanced squamous carcinoma of the head and neck. *Semin Oncol* 1985;12:71–78.

57. Iosilevsky G, Front D, Bettman L, et al. Uptake of gallium-67 citrate and (2-3H)deoxyglucose in the tumor model, following chemotherapy and radiotherapy. *J Nucl Med* 1985;278–282.

58. Bichel P, Hansen HH. The incorporation of 67Ga in normal and malignant cells and its dependence on growth rate. *Br J Radiol* 1972;45:182–184.

59. Higashi T, Kobayashi M, Wakao H, Jinbu Y. The relationship between 67Ga accumulation and ATP metabolism in tumor cells in vitro. *Eur J Nucl Med* 1989;15:152–156.

60. Abe Y, Matsuzawa T, Fujiwara T, et al. Assessment of radiotherapeutic effects on experimental tumors using 18F-2-fluoro-2-deoxy-D-glycose. *Eur J Nucl Med* 1986;12:325–328.

61. Brauneis JW, Laskawi R, Schröder M, Göhde W. Ergebnisse der Impulscytophotometrie bei malignen Tumoren des Kopf-Hals- Bereiches. *HNO* 1987;37:369–372.

62. Watanabe A, Tanaka R, Takeda N, Washiyama K. DNA synthesis, blood flow, and glucose utilization in experimental rat brain tumors. *J Neurosurg* 1989;70:86–91.

63. Minn H, Joensuu H, Ahonen A, Klemi P. Fluorodeoxyglucose imaging: a method to assess the proliferative activity of human cancer in vivo. Comparison with DNA flow cytometry in head and neck tumors. *Cancer* 1988;61:1776–1781.

64. Flier J, Mueckler MM, Usher P, Lodish HF. Elevated levels of glucose transport and transporter messenger RNA are induced by ras or src oncogenes. *Science* 1987;235:1492–1495.

65. Persons DA, Schek N, Hall BL, Finn OJ. Increased expression of glycolysis-associated genes in oncogene-transformed and growth-accelerated states. *Molecular Carcinogenesis* 1989;2:88–94.

66. McLoud TC, Kosiuk JP, Templeton PA, et al. CT in the staging of bronchogenic carcinoma: update of analysis by correlative lymph node mapping and sampling [Abstract]. *Radiology* 1989;173(P):69.

67. Webb WR, Gatsonis CA, Zerhouni EA, et al. Comparison of CT and MR imaging in lung cancer staging: preliminary results of the RDOG imaging study [Abstract]. *Radiology* 1989;173(P):69.

68. Nolop KB, Rhodes CG, Brudin LH, et al. Glucose utilization in vivo by human pulmonary neoplasms. *Cancer* 1987;60:2682–2687.

69. Knopp MV, Strauss LG, Dimitrakopoulou A, et al. Comparison of PET with F-18 deoxyglucose and CT in imaging of lung tumors [Abstract]. *Radiology* 1989;173(P):69–70.

70. Kubota K, Matsuzawa T, Fujiwara T, et al. Comparison of C-11 methionine and F-18 fluorodeoxyglucose for the differential diagnosis of lung tumor. *J Nucl Med* 1989;30:788–789.

71. Strauss LG, Clorius JH, Manke H, et al. Positronemissionstomographie (PET) von Lungentumoren. *Nucl Med* 1988;27:9–10.

72. Strauss LG. Aktueller Stand des Klinischen Einsatzes der Positronen-Emissions-Tomographie (PET). *Zbl Rad* 1989;138:756.

73. Knopp MV, Strauss LG, Haberkorn U, et al. Use of positron emission tomography for optimized therapy management of patients with lung tumors. *Eur J Nucl Med* 1990;16:560.

74. Knopp MV, Strauss LG, Haberkorn U, et al. Positron emission tomography (PET) with F-18-deoxyglucose in the imaging and staging of bronchogenic carcinoma. *Eur J Nucl Med* 1990;16:560.

75. Knopp MF, Strauss LG, Haberkorn U, et al. PET of the thorax: assessment of its clinical application in tumor staging. *Radiology* 1990;177:174.

76. DiChiro G, Dela Paz RL, Brooks RA, et al. Glucose utilization of cerebral gliomas measurement by (18F)fluorodeoxyglucose and positron emission tomography. *Neurology* 1982;32:1323–1329.

77. DiChiro G. Positron emission tomography using [18F]fluorodeoxyglucose in brain tumors: a powerful diagnostic and prognostic tool. *Invest Radiol* 1986;22:360–371.

78. Alavi JB, Alavi A, Chawluk J, et al. Positron emission tomography in patients with glioma: a prediction of prognosis. *Cancer* 1988;62:1074–1078.

79. Francavilla TL, Miletich RS, Dichiro G, et al. Positron emission tomography in the detection of malignant degeneration of low-grade gliomas. *Neurosurgery* 1989;24:1–5.

80. Tyler JL, Diksic M, Villemure J-G, et al. Metabolic and hemodynamic evaluation of gliomas using positron emission tomography. *J Nucl Med* 1987;28:1123–1133.

81. DiChiro G, Hathaway J, Katz DA, et al. Glucose utilization by intracranial meningiomas as an index of tumor aggressivity and possibility of recurrence: a PET study. *Radiology* 1987;164:521–526.

82. DiChiro G, Oldfield E, Wright DC, et al. Cerebral necrosis after radio-

therapy and for intraarterial chemotherapy for brain tumors: PET and neuropathologic studies. *AJNR* 1987;8:1083–1091.

83. Valk PE, Budinger TF, Levin VA, et al. PET of malignant cerebral tumors after interstitial brachytherapy: demonstration of metabolic activity and correlation with clinical outcome. *J Neurosurg* 1988;69:830–838.

84. Mineura K, Yasuda T, Sasajima T, et al. Clinical significance of F-18-fluorodeoxyglucose positron emission tomography in brain tumors. European Workshop on FDG in Oncology. Heidelberg, Germany, June 15–16, 1990.

85. Grossman SA, Eller S, Dick J, et al. Thymidine, leucine and 2-deoxyglucose incorporation in brain tumors and abscess: a quantitative autoradiographic (QAR) study with implications for PET scans. *Ann Proc Am Assoc Cancer Res* 1988;29:516.

86. O'Tuama LA, Guilarte TR, Douglass KH, et al. Assessment of [11C]-L-methionine transport into the human brain. *J Cereb Blood Flow Metab* 1888;8:341–345.

87. Ericson K, Lilja A, Bergström M, et al. Positron emission tomography with ([11C]methyl)-L-methionine [11C]D-glucose, and [68Ga]EDTA in supratentorial tumors. *J Comput Assist Tomogr* 1895;9:683–689.

88. Ogawa T, Shishido F, Kanno I, et al. Values of PET for diagnosis of recurrent brain tumor and radiation necrosis. European Workshop on FDG in Oncology. Heidelberg, Germany, June 15–16, 1990.

89. Foster DO, Pardee AB. Transport of amino acids by confluent and nonconfluent 3T3 and polyoma virus-tramsformed 3T3 cells growing on glass cover slips. *J Biol Chem* 1969;244:2675–2681.

90. Isselbacher KJ. Sugar and amino acid transport by cells in culture: Differences between normal and malignant cells. *N Engl J Med* 1972;286:929–933.

91. Johnstone RM, Scholefield PG. Amino acid transport in tumor cells. *Adv Cancer Res* 1965;9:143–226.

92. Parnes JR, Isselbacher KJ. Transport alterations in virus transformed cells. *Prog Exp Tumor Res* 1978;22:79–122.

93. Hübner KF, Krauss S, Washburn LC, et al. Tumor detection with 1-aminocyclopentane and 1-aminocyclobutane C-11-carboxylic acid using positron emission computerized tomography. *Clin Nucl Med* 1981;6:249–252.

94. Bergström M, Muhr C, Lundberg PO, et al. Amino acid distribution and metabolism in pituitary adenomas using positron emission tomography with D-[11C]methionine and L-[11C]methionine. *JCAT* 1987;11:384.

95. Hübner KF, Smith GT, Goodman MM, et al. Dynamic FDG and amino acid PET for assessment of tumor proliferation. European Workshop on FDG in Oncology. Heidelberg, Germany, June 15–16, 1990.

96. Lilja A, Bergström K, Hartvig P, et al. Dynamic study of supratentorial gliomas with L-methyl-11C-methionine and positron emisson tomography. *AJNR* 1985;6:505–514.

97. Hüber KF, Parvis JT, Mahaley SM, et al. Brain tumor imaging by positron emission computed tomography using 11C-labeled amino acids. *J Comput Assist Tomogr* 1982;6:544–550.

98. Meyer G-J, Harre R, Orth F, et al. In vivo protein synthesis in human brain tumors measured with 11C-L-methionine. *J Nucl Med* 1989;30:910–911.

99. Schmall B, Conti PS, Bigler RE, et al. Synthesis and quality assurance of C-11-alpha-aminoisobutyric acid (AIB), a potential radiotracer for imaging and amino acid transport studies in normal and malignant tissues. *Int J Nucl Med Biol* 1984;3/4:209–214.

100. Hayes RL, Washburn LC, Wieland BW, et al. Carboxyl-labeled 11C-1-aminocyclopentane carboxylic acid, a potential agent for cancer detection. *J Nucl Med* 1976;17:748–751.

101. Bergström M, Muhr C, Ericson K, et al. Normal pituitary examined with positron emission tomography and (methyl-11C)-L-methionine and (methyl-11C)-D-methionine. *Neuroradiology* 1978;29:221.

102. Bergström M, Muhr, C, Lundberg PO, et al. Rapid decrease in amino acid metabolism in prolactin-secreting pituitary adenomas after bromocriptine treatment: a PET study. *JCAT* 1978;11:815.

103. Hiesiger E, Follwer JS, Wolf AP, et al. Serial PET studies of human cerebral malignancy with [1-11C]putrescine and [1-11C]2-deoxy-D-glucose. *J Nucl Med* 1987;28:1251–1261.

104. Thomas G, Szücs M, Mamone JY, et al. Sigma and opioid receptors in human brain tumors. *Life Sciences* 1990;46:1279–1286.

105. Sundoro-Wu BM, Schmall B, Conti PS, et al. Selective alkylation of pyrimidyl-dianions: synthesis and purification of 11C-labeled thymidine for tumor visualization using positron emission tomography. *Int J Radiat Isot* 1984;35:705–708.

106. Conti PS, Grossman SA, Wilson AA, et al. Brain tumor imaging with C-11-labeled thymidine and PET. *Radiology* 1990;177P:234.

107. Paul R. Comparison of fluorine-18-2-fluorodeoxyglucose and gallium-67 citrate imaging for detection of lymphoma. *J Nucl Med* 1987;28:288–292.

108. Kuwabara Y, Ichiya Y, Otsuka M, et al. High [18]FDG uptake in primary cerebral lymphoma: A PET study. *J Comput Assist Tomogr* 1988;12:47–48.

109. Yoshikawa K, Okada J, Uno K, et al. Evaluation of therapeutic effect on the malignant lymphoma by dynamic positron emission tomographic technique using fluorine-18 2-deoxy-2-fluoro-D-glucose. *J Nucl Med* 1989;30:910.

110. Okada J, Joshikawa K, Imazeki K et al. Comparison of fluorine-18 FDG and gallium-67 in malignant lymphoma. *J Nucl Med* 1990;31:888.

111. Leskinen-Kallio S, Ruotsalainen U, Teräs M, et al. The uptake of [11C] methionine and FDG in non-Hodgkins lymphoma. European Workshop on FDG in Oncology. Heidelberg, Germany, June 15–16, 1990.

112. Martiat Ph, Ferrant A, Labar D, et al. In vivo measurement of carbon-11-thymidine uptake in non-Hodgkins lymphoma using positron emission tomography. *J Nucl Med* 1988;29:1633–1637.

113. Shields AF, Kozell LB, Links JM, et al. Comparison of PET imaging using [11C]thymidine labeled in the ring-2 and methyl positions. *J Nucl Med* 1990;31:794.

114. Conti PS, Sordillo PP, Schmall B, et al. Tumor imaging with carbon-11-labeled alpha-aminoisobutyric acid (AIB) in a patient with advanced malignant melanoma. *Eur J Nucl Med* 1986;12:352–356.

115. Conti PS. Application of radiolabeled metabolic probes for tumor imaging. Correlative animal and human PET studies using F-18-fluorodeoxyglucose. C-11-thymidine, and C-11-amino acids. European Workshop on FDG in Oncology. Heidelberg, Germany, June 15–16, 1990.

116. Strauss LG, Tilgen W, Dimitrakopoulou A, et al. PET studies with F-18-deoxyglucose (FDG) in patients with metastatic melanoma prior to and after therapy. *J Nucl Med* 1990;31:804.

117. Sordillo PP, DiResta E, Conti PS, et al. Imaging studies using C-11-alpha-aminoisobutyric acid (AIB) in patients with malignant melanoma. *J Nucl Med* 1988;29:904.

118. Wahl RL, Cody R, Hutchins G. FDG PET of breast cancer: imaging and monitoring the response to treatment. European Workshop on FDG in Oncology. Heidelberg, Germany, June 15–16, 1990.

119. Wahl RL, Cody R, Hutching G, et al. Sequential quantitative FDG/PET assessment of the metastatic response of breast carcinomas to chemohormonotherapy [Abstract]. *J Nucl Med* 1990;31:746.

120. Wahl RL, Cody R, Hutchins G, Mudgett E. Positron emission tomographic (PET) scanning of primary and metastatic breast carcinoma with the radiolabeled glucose analog 2-[18F]-fluoro-deoxy-2-D-glucose (FDG): initial clinical evaluation. *Radiology* 1991: in press.

121. Mintun MA, Welch MJ, Siegel BA, et al. Breast cancer: PET imaging of estrogen receptors. *Radiology* 1988;169:45–48.

122. McGuire AH, Lyss AP, Brodack JW, et al. Positron tomographic assessment of 16-alpha-[F-18]-fluoroestradiol (FES) uptake in metastatic breast carcinoma: effect of antiestrogen therapy. *J Nucl Med* 1989;30:788.

123. Dehdarsti F, Mcguire AH, Van Brocklin HF, et al. Assessment of progestin receptors in breast carcinoma by positron emission tomography. *J Nucl Med* 1990;31:746.

124. Gelbard AS, Clark LP, McDonald JM, et al. Enzymatic synthesis and organ distribution studies with 13N-labeled L-glutamine and L-glutamic acid. *Radiology* 1975;116:127–132.

125. Gelbard AS, Benua RS, Laughlin JS, et al. Quantitative scanning of osteogenic sarcoma with nitrogen-13-labeled L-glutamate. *J Nucl Med* 1979;20:782–784.

126. Reiman RE, Huvos AG, Benua RS, et al. Quotient imaging with N-13 glutamate in osteogenic sarcoma. *Cancer* 1981;48:1976–1981.

127. Reiman RE, Rosen G, Gelbard AS, et al. Imaging of primary Ewing sarcoma with N-13-L glutamate. *Radiology* 1982;142:495–500.

128. Schmall B, Conti PS, Bigler RE, et al. Imaging studies of patients with malignant fibrous histiocytoma using C-11-alpha-aminoisobutyric acid (AIB). *Clin Nucl Med* 1987;1:22–26.

129. Bigler RE, Zanzonico PB, Schmall B, et al. Evaluation of [1-C-11]-alpha-aminoisobutyric acid for tumor detection and amino acid transport measurements: Spontaneous canine tumor studies. *Eur J Nucl Med* 1985;10:48–55.

130. Kern KA, Brunetti A, Norton JA, et al. Metabolic imaging of human extremity musculoskeletal tumors by PET. *J Nucl Med* 1988;29:181–186.

131. Griffeth LK, Dehdashti F, McGuire AH, et al. PET evaluation of soft-tissue masses with F-18-fluorodeoxyglucose. *J Nucl Med* 1990;31:746.

132. Adler LP, Blair HF, Makley JT, et al. Correlation of FDG uptake with tumor grade in musculoskeletal tumors. *J Nucl Med* 1990;31:756.